Bulletin of the Seismological Society of America, Vol. 108, No. 2, pp. 781–800, April 2018, doi: 10.1785/0120170002

Seismic Hazard, Risk, and Design for South America

by Mark D. Petersen, Stephen C. Harmsen, Kishor S. Jaiswal, Kenneth S. Rukstales, Nicolas Luco, Kathleen M. Haller, Charles S. Mueller, and Allison M. Shumway

Abstract We calculate seismic hazard, risk, and design criteria across South America using the latest data, models, and methods to support public officials, scientists, and engineers in earthquake risk mitigation efforts. Updated continental scale seismic hazard models are based on a new seismicity catalog, seismicity rate models, evaluation of earthquake sizes, fault geometry and rate parameters, and ground-motion models. Resulting probabilistic seismic hazard maps show peak ground acceleration, modified Mercalli intensity, and spectral accelerations at 0.2 and 1 s periods for 2%, 10%, and 50% probabilities of exceedance in 50 yrs. Ground shaking soil amplification at each site is calculated by considering uniform soil that is applied in modern building codes or by applying site-specific factors based on V_{S30} shear-wave velocities determined through a simple topographic proxy technique. We use these hazard models in conjunction with the Prompt Assessment of Global Earthquakes for Response (PAGER) model to calculate economic and casualty risk. Risk is computed by incorporating the new hazard values amplified by soil, PAGER fragility/vulnerability equations, and LandScan 2012 estimates of population exposure. We also calculate building design values using the guidelines established in the building code provisions. Resulting hazard and associated risk is high along the northern and western coasts of South America, reaching damaging levels of ground shaking in Chile, western Argentina, western Bolivia, Peru, Ecuador, Colombia, Venezuela, and in localized areas distributed across the rest of the continent where historical earthquakes have occurred. Constructing buildings and other structures to account for strong shaking in these regions of high hazard and risk should mitigate losses and reduce casualties from effects of future earthquake strong ground shaking. National models should be developed by scientists and engineers in each country using the best available science.

Introduction

In this article, we assess the seismic hazard across South America by applying methods from the U.S. Geological Survey (USGS) National Seismic Hazard Models (NSHMs), seismic risk using the guidelines of the Prompt Assessment of Global Earthquakes for Response (PAGER), and seismic design criteria by implementing the National Earthquake Hazards Reduction Program (NEHRP) seismic design criteria (Wald *et al.*, 2008; Jaiswal *et al.*, 2014; Petersen *et al.*, 2014; Luco *et al.*, 2015). The purpose of these maps is to provide information for scientists, engineers, and public policy officials that may be helpful in making decisions regarding earthquake hazard and risk mitigation strategies and to initiate discussions on building code design procedures. Policy applications for individual countries should incorporate additional information from the local science and engineering experts who have more regional information and experience. This regional South America model may serve as a useful comparison with these other more detailed models that are developed within each country.

Over the past century, many large earthquakes along subduction zones, within the downgoing subducting plates and in the shallow crust, have resulted in great losses across South America. For example, earthquakes over the past century have caused significant damage and tens of thousands of casualties across the northern and western part of the continent, including the following earthquakes: 1906 moment magnitude (**M**) 8.4 Ecuador earthquake, 1922 **M** 8.3 Chile earthquake, 1939 **M** 7.8 Chile earthquake, 1944 **M** 7.0 Argentina earthquake, 1946 **M** 6.8 Peru earthquake, 1949 **M** 6.5 Ecuador earthquake, 1960 **M** 9.5 Chile earthquake, 1970 **M** 7.9 Peru earthquake, 1987 **M** 7.1 Colombia earthquake, 1999 **M** 6.1 Colombia earthquake, 2007 **M** 8.0 Peru earthquake, and 2010 **M** 8.8 Chile earthquake (see Data and Resources). Figure 1 shows large potentially damaging earthquakes

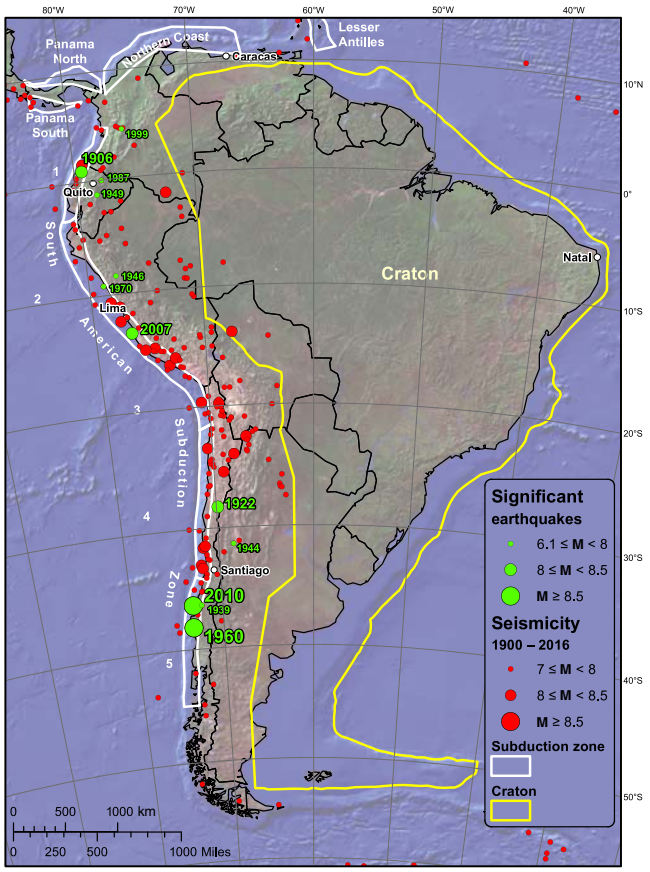

Figure 1. Modeled subduction interface zones 1–5, craton-South America Plate, circles depict large earthquakes ($\mathbf{M} \geq 7$) since 1900, significant earthquakes labeled by date. Five cities where deaggregations were calculated are identified. The color version of this figure is available only in the electronic edition.

($\mathbf{M} \geq 7$) across South America and highlights the damaging earthquakes described above. A probabilistic seismic hazard analysis can be incorporated into building codes to ensure that strong ground shaking provisions are considered in design procedures for seismically active areas. Seismic procedures require stronger buildings in places where earthquakes are common to increase seismic safety, while conserving resources in places where earthquakes are infrequent.

Seismic hazard assessments forecast the potential earthquake locations, earthquake rates, and ground-shaking levels and are used as input data for risk assessments and seismic design criteria. Typically, the earthquake source models are based on Poisson statistics that are time invariant, but time-dependent models can also be generated when the date of the most recent earthquake is known or inferred on individual seismic sources. Earthquake rates and locations can be assessed using the geologic or geodetic-based fault-slip rates or paleoseismic rates of large earthquakes interpreted from fault-trenching studies. A seismicity catalog provides another dataset used to forecast future earthquakes. Seismicity-based models rely on the assumption that small-to-moderate size earthquakes are located where future large earthquakes are more likely to occur. These seismicity-based models are more robust in places with intense seismicity; however, in low-seismicity areas the models account for hazard where moderate-size events have occurred in the past or across a zone where seismicity and tectonic characteristics are similar. To develop such models, seismicity (1964–2013) with $\mathbf{M} \geq 5$ is smoothed spatially to calculate earthquake productivity levels over a gridded area. For both fault- and seismicity-based models, we apply a doubly truncated Gutenberg and Richter (1944) magnitude–frequency distribution to estimate the rates of different sizes of earthquakes. The distribution starts at a minimum earthquake magnitude (M_{min}) that is known to cause building damage and terminates at a maximum magnitude (M_{max}) that is thought to be the largest earthquake that can affect the region. This M_{max} is obtained from global observations of the largest earthquakes in analogous tectonic regions or a magnitude consistent with the size of the largest historical regional earthquake along with additional consideration of uncertainties. Ground-shaking hazard is assessed by applying ground-motion models (GMMs) for different types of shaking (e.g., peak ground acceleration [PGA] and spectral acceleration [SA]), which are developed from strong-motion data and numerical modeling. The hazard analysis results in hazard curves that show the probability or rate of exceeding various ground-motion levels.

In June 2016, the United States Agency for International Developments Office of U.S. Foreign Disaster Assistance sponsored a USGS-University of Chile workshop (in Coast Rica) in which 24 scientists from 17 countries across South America, Central America, and the Caribbean evaluated available hazard models, assessed the need for future seismic hazard and risk assessments, and discussed products that would be most useful in mitigating future earthquake damage and loss. Attendees indicated that they would appreciate international cooperation in developing continental-based hazard maps but emphasized that scientists from each country should be responsible for developing maps and hazard products for national and local government use. They also suggested that additional training and hazard-based workshops would help standardize methodologies and reduce border discrepancies. This suggestion relates to one of the most challenging issues in hazard assessment: developing standardized and harmonized datasets across regions and borders that can be applied consistently in assessing hazard. The science community should encourage studies and projects that promote this standardization. Attendees agreed that improved hazard assessment and seismic monitoring would also promote cooperation among scientists. In addition, they provided specific advice for improving the hazard and risk models. This information was considered in updating the USGS hazard, exposure, risk, and design maps described here.

In this article, we present a new continental scale seismic hazard assessment for South America developed by the USGS using the latest seismicity, fault, ground-motion data, and new methodologies applied in the USGS NSHMs. We use this hazard model to assess the PAGER risk assessments

and NEHRP design criteria. The amount of information needed to define these models and the number of output products is very large; therefore, we will show selected results in this article and all other source model components (e.g., seismicity catalogs, *a*-values for background seismicity [agrids], the hazard input document [HID], and source code input files) and results (e.g., hazard curves, hazard maps, deaggregation plots, and risk and design values) may be obtained from ScienceBase (see Data and Resources). This sensitivity of hazard to various alternative input parameters is described in Petersen *et al.* (2017).

Previous Studies and Approaches

Efforts to assess seismic hazard and risk across the continent have been ongoing since at least 1985 when the Regional Center for Seismology for South America (CERESIS) released a historical maximum intensity map for a 460-yr period from 1520 to 1981 (see Data and Resources). Probabilistic seismic hazard assessments were initially conducted by the Global Seismic Hazard Assessment Program (GSHAP), which released a worldwide seismic hazard map in 1999 that provided estimates of PGA for a 10% probability of exceedance in 50-yr hazard level (Tanner and Shepherd, 1997; Dimate *et al.*, 1999; Giardini *et al.*, 1999; Shedlock, 1999; Shedlock and Tanner, 1999). This global map involved projecting historical seismicity to estimate future earthquake rates.

Shortly after this 1999 hazard map was released, CERESIS invited the USGS to assess seismic hazard at different return periods and ground-motion types. In addition, they wanted the USGS to incorporate fault information into the hazard model using probabilistic methodologies, data, and models applied in the USGS NSHMs (Petersen *et al.*, 2008). The resulting fault- and seismicity-based hazard model for South America (referred to as the 2010 USGS model, see Data and Resources) was implemented in the first Global Earthquake Model (GEM; Pagani *et al.*, 2010).

Several other groups have updated the South America model. GEM has recently updated the hazard and risk models for implementation in the recent South America Risk Assessment project (see Data and Resources). CERESIS has recently released their first preliminary South America probabilistic seismic hazard assessment for 10% probability of exceedance in 50- and 100-yr levels that is based on shallow and intermediate depth historical earthquakes and multiple ground-motion models (Tavera *et al.*, 2015). Proprietary models have also been produced by companies involved in insurance and risk mitigation. In addition to the continental scale hazard assessments, several regional or local models have also been developed (e.g., Beauval *et al.*, 2013, 2014, for Quito, Ecuador; Medina *et al.*, 2017, for Chile). Assessments of seismic hazard by different practitioners allow for better quantification of the uncertainties in the hazard analysis and provide checks on the calculations and inputs.

Seismic hazard assessments that incorporate amplification of soils are used along with the vulnerability equations and population density (which serves as a proxy for infrastructure inventory) to quantify the aggregate risk across regions. Several hazard and risk assessments have been produced over the past two decades. Nevertheless, seismic risk assessments for South America have not been commonly available in the public domain until the last decade or so as new soils maps, inventory, and methodologies were developed. The USGS recently assessed the risk for South America using the methodology of PAGER and the 2010 USGS hazard model (Earle *et al.*, 2009; Jaiswal *et al.*, 2014). GEM recently assessed risk across this region using a more thorough consideration of buildings (see Data and Resources). Several proprietary models have also been developed to guide insurance and risk assessments across the continent, but these models are not generally available for the public to apply in risk mitigation planning. These models provide policy makers estimates of economic and casualty losses and can provide information for discussions on risk mitigation and resilience of communities.

One of the most important ways to achieve seismic safety is through properly defining the building standards in regions with seismic activity. Building codes have been in place for many decades at various locations across the globe and these codes are continually updated as new information on seismic shaking becomes available. For example, the seismic design provisions in the United States incorporate methods and data developed by the Building Seismic Safety Council (BSSC) as part of the NEHRP Recommended Seismic Provisions and the American Society of Civil Engineers (ASCE) 7 Standard updates (Luco *et al.*, 2015); these provisions are typically updated every 6 yrs. Building codes have taken various forms and considered different ground-motion types and hazard levels (e.g., maximum modified Mercalli intensity [MMI], response spectra, and PGA at 2%, 5%, or 10% probability of exceedance in 50 yrs). Starting with the 2009 NEHRP Recommended Seismic Provisions, the BSSC applied risk targeted maximum considered earthquake (MCE_R) spectral response accelerations for 0.2 and 1 s SA with 5% damping and for a site condition defined by a time-averaged shear-wave velocity in the upper 30 m (V_{S30}) of 760 m/s. The design criteria were produced having a risk target consistent with a 1% chance of building collapse in a 50-yr period for the purpose of designing buildings and other structures. Seismic ground motions applied in design rely on the probabilistic hazard curves that incorporate uncertainties, but also depend on simple scenario (deterministic) 84th-percentile ground motions that constrain the larger ground motions to levels acceptable by engineers. We develop these design products using methodologies applied in international building codes for use by public policy officials in discussions regarding earthquake safety because no such criteria have been available for South America up to the present.

In this article, we discuss updates of the seismic hazard, risk, and building code models. These models can inform the

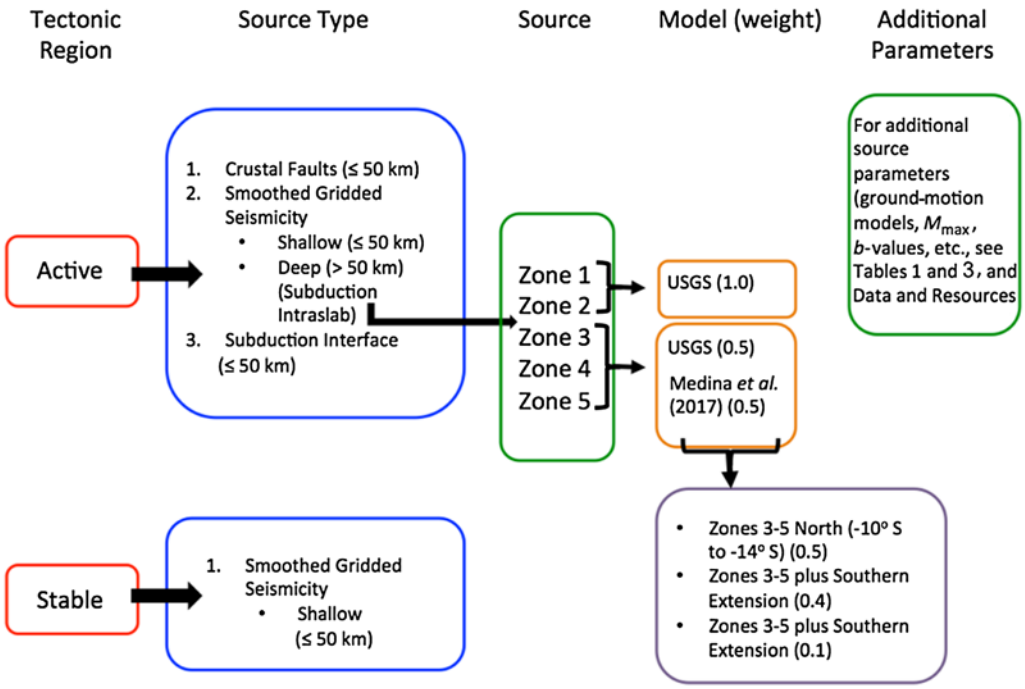

Figure 2. A simplified logic tree for the 2017 U.S. Geological Survey (USGS) South America model (for more information and additional source parameters, see Data and Resources). The color version of this figure is available only in the electronic edition.

user community in making important risk mitigation and seismic safety decisions.

Seismic Hazard Model

The updated USGS South American model presented here (referred to as the 2017 USGS South America model) is based on a smoothed (gridded) seismicity model, a subduction model, crustal fault model, and GMMs that are described below and apply the probabilistic seismic hazard methodology of Cornell (1968). These models are combined to account for ground shaking from earthquakes on known faults as well as earthquakes on faults not included in the model (Moschetti *et al.*, 2015; Petersen *et al.*, 2015; Rezaeian *et al.*, 2015). Figure 2 shows a simplified logic tree for the 2017 USGS South America model (for more information and additional source parameters, see Data and Resources).

Smoothed Seismicity Model

The smoothed seismicity model first requires the development of a uniform moment-magnitude seismicity catalog that can be used to assess the location and rate of future earthquakes. We use the International Seismological Centre-GEM (ISC-GEM) Global Instrumental Earthquake Catalogue through 2013. The ISC-GEM earthquake catalog was developed by relocating all events between 1900 and 2013, with a special focus on the depth of earthquakes. Typically, we remove known mine blasts or man-made-induced earthquakes for the long-term analysis, but this analysis has not been considered here due to lack of information on these processes. For example, there are known induced earthquakes in Colombia that should be considered in future analyses. Uncertainties in the locations of the earthquakes have error ellipses of about 105 km^2 and are on the order of 10 km laterally and less than 15 km in depth for many of the earthquakes; this effort represents the best available science in our assessment of earthquake locations as described by Bondar *et al.* (2015). For the following statistics and analyses, we supplemented the ISC-GEM catalog by adding new earthquakes between January 2014 and September 2016 from the Advanced National Seismic System Comprehensive Earthquake Catalog (ComCat; see Data and Resources). The earthquakes in the catalog are mostly located along the western and northern coasts with deeper seismicity beneath the inland areas (Fig. 3).

We decluster the catalog by removing foreshocks and aftershocks (following the method outlined by Gardner and Knopoff, 1974) so that only independent events are considered, as required in the probabilistic methodology (Cornell, 1968; Frankel *et al.*, 1996; Petersen *et al.*, 2008, 2014, 2015). This declustering of the catalog allows for the long-term assessment of hazard and does not account for the high short-term rates associated with aftershocks. The full seismicity catalog contains 20,525 events with $\mathbf{M} \geq 5$. After declustering the catalog, 9115 events remain, more than a 50% decrease (Fig. 3). Figure 4 shows the number of earthquakes in each of the different source zones that cover South America. Several thousand earthquakes are deeper than 50 km (3041) or are in shallow crustal areas outside of the subduction zone (4408). About a thousand (1107) earthquakes are located in the upper 50 km near the subduction interface; several of these

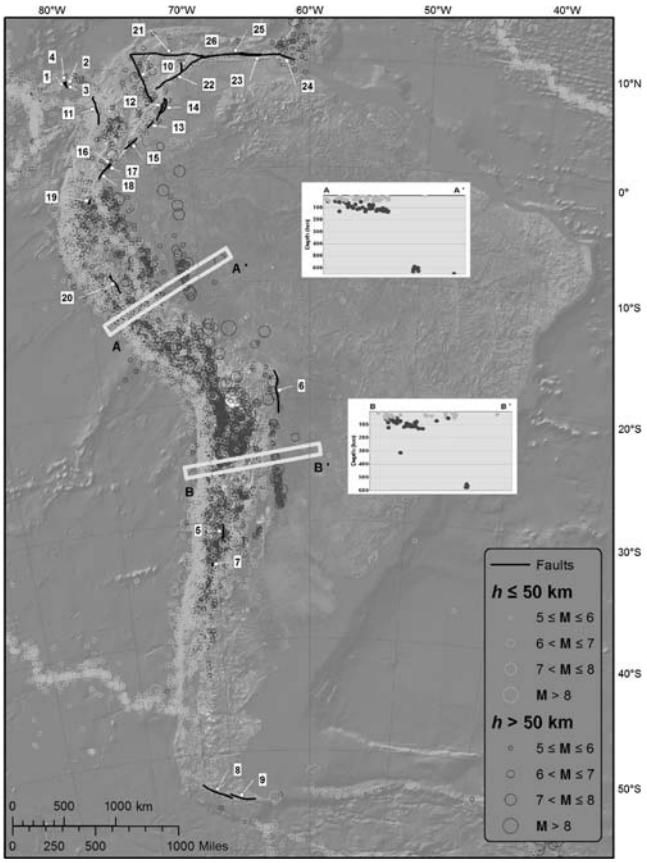

Figure 3. Map showing earthquakes in the updated catalog (declustered catalog), faults applied in model shown as solid lines (number corresponds to number of fault in Table 1), and two cross sections showing seismicity and depth. The color version of this figure is available only in the electronic edition.

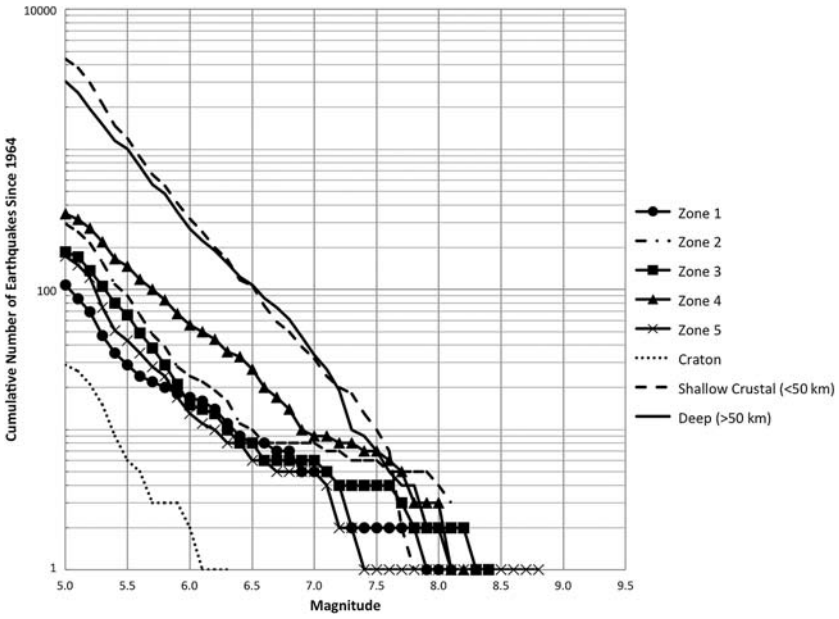

Figure 4. Cumulative number of earthquakes as a function of magnitude for the five subduction interface zones, craton, other shallow crustal areas, and for deeper earthquakes (depth > 50 km). The catalog shows earthquakes between 1964 and 2016.

earthquakes have magnitudes that are greater than **M** 7.0 and some are greater than **M** 8.0 and 9.0.

We assess earthquake rates for each magnitude considered in the analysis by estimating completeness levels and *b*-values, counting historical earthquakes in 0.1°-by-0.1° cells, and applying a double truncated magnitude–frequency distribution to estimate future seismicity rates (see Data and Resources). Earthquakes with **M** ≥ 5.4 since 1964, **M** ≥ 5.0 since 1969, and **M** ≥ 4.5 since 2000 are applied in this region. Gridded earthquake rates are smoothed using a fixed-length 50 km smoothing kernel similar to the Petersen *et al.* (2008, 2014, 2015) models. Separate rate models are developed for craton (stable continental regions) and active tectonic regions. The earthquakes are spatially smoothed, with earthquake depths between 0 and 50 km (shallow crustal) and earthquakes with depths greater than 50 km (deep intraslab) smoothed separately. We use the gridded rates (10^a) along with an estimate of slope of the Gutenberg and Richter distribution (*b*-value) and truncation levels of the magnitude–frequency distribution to forecast earthquakes in the model (Gutenberg and Richter, 1944). For the gridded seismicity model, we apply region- and depth-dependent *b*-values that range from 0.9 to 0.95 based on the Weichert (1980) methodology. We truncate the magnitude–frequency distribution at M_{min} of 5.0 and an M_{max} that depends on the region. For the active crustal region, we apply M_{max} of 7.8. This M_{max} is chosen to account for large earthquakes that are not on known faults; however, the value is quite uncertain and should be further analyzed in future assessments. For the craton region, the main weights are given to earthquakes with M_{max} between **M** 7.1 and 7.4. This is analogous with the mean values applied in the cratonic region of the United States and are based on compilations of global earthquakes (Petersen *et al.*, 2014). The M_{max} distributions are broad and generally are similar to the M_{max} distribution we used for the 2014 NSHM (Petersen *et al.*, 2014, 2015). Table 1 summarizes the source parameters for the smoothed seismicity model.

Subduction Model

Most of the largest earthquakes in the historical catalog are located on or near the subduction zones: along the subduction interface, intraslab, and within the outer rise offshore of the trench. We consider the subduction zones off the northern and western coasts of South America, the Panama deformation zones, as well as the Lesser Antilles subduction zone in this hazard assessment. In this section, we discuss the characterization of large earthquakes on the subduction interface (**M** 7.5–9.5). Shallow crustal (≤ 50 km) and deep earthquakes (> 50 km) with

Table 1
Summary of Source Model Parameters

Source Type	Source Name
Crustal fault model—depth < 50 km	(1) Azota fault, (2) Pedro Miguel fault, (3) Pedro Miguel-Limon fault, (4) Rio Gatun fault, (5) El Tigre fault, (6) Mandeyapecua fault, (7) San Ramon fault, (8) Lago Fagnano fault W*, (9) Lago Fagnano fault E†, (10) Santa Maria–Bucamuga fault System, (11) Bahia Solano fault, (12) North Guaicaramo fault, (13) South Guaicaramo fault, (14) Yopal fault, (15) Algeciras fault, (16) Sibundoy fault, (17) Afiladores fault, (18) Chingual fault, (19) Pallatanga fault, (20) Cordillera Blanca fault zone, (21) Oca-Ancon fault, (22) Boconó fault, (23) El Pilar fault, (24) Los Bajos fault, (25) San Sebastian fault, (26) Burbusay fault, Quito zone, and Valencia zone
Smoothed (gridded) seismicity model—shallow depth < 50 km, deep depth 50–200+ km	Shallow active crustal regions: South America grid and South America east
	Shallow stable craton regions: South America craton
	Deep (intraslab): South America deep
Subduction Model (Interface)—depth < 50 km	North Panama deformation zone
	South Panama deformation zone
	Lesser Antilles subduction zone
	North Coast subduction zone
	Zone 1
	Zone 2
	Zone 3
	Zone 4
	Zone 5
	Zones 4 and 5
	Zones 3–5 N (−10° S to −14.9° S) Medina *et al.* (2017)
	Combo zones 3–5 plus southern extension Medina *et al.* (2017)
	Combo zones 3–5 plus southern extension Medina *et al.* (2017)

*Western section.
†Eastern section.

magnitudes less than **M** 7.5 are characterized using the smoothed seismicity model described above. This transition between the shallow and deep seismicity is typically between 30 and 70 km depth, which generally corresponds to the thickness of the continental crust and to the depth limit of most subduction interface earthquakes. Many of these deep earthquakes are most likely located within the Wadati–Benioff zone as a result of the downgoing slab stresses associated with the subduction zone.

For this subduction model analysis, we apply the Slab 1.0 model fault geometry to account for the locations of subduction zones along the west coast of South America and along the Lesser Antilles of the Caribbean (Hayes *et al.*, 2012; Fig. 1). This model is a 3D compilation of subduction geometries determined from historic earthquakes, centroid moment tensor solutions, seismic reflection data, global plate models, bathymetry, and sediment thickness information that defines the geometry of the subducting slab. The northern coast subduction was modeled based on the bathymetric data similar to the model of Bird (2003). We also considered the Panama deformation zones that were digitized based on regional geological maps and bathymetry maps (M. Petersen *et al.*, unpublished manuscript, 2005, see Data and Resources).

A primary contributor to hazard is the South American subduction zone off the western coast of South America that accommodates subduction of the Nazca plate beneath the South American plate margin (Figs. 1 and 3). We separated the subduction interface down to 50 km depth into five zones based on locations of impinging subducting ridges, dimensions of large earthquakes, and fault complications (fault bends, splays, and stepovers) (Figs. 1 and 3). All five zones have experienced earthquakes greater than **M** 8.0 during the past century. Zones 2 and 4 have the highest rate of earthquakes. Zone 5 hosted the 1960 **M** 9.5 southern Chile and the 2010 **M** 8.8 Maule earthquakes.

Earthquake rates and geometry for the five subduction source zones are shown in Figures 4 and 1, respectively. These subduction interface rates are based on the observed historical catalog of $\mathbf{M} \geq 7$ earthquakes in each of the zones considered in the analysis. For this assessment, we consider earthquakes since 1900, but we also examined the catalog that extends back to the 1400s for consistency. The portion of the catalog prior to 1900 is very incomplete and only contains very uncertain locations and magnitudes for a few selected earthquakes, so it is difficult to model rates based on these data. Nevertheless, it may be important to consider these earlier earthquake data in site-specific analyses.

To model the rate of large earthquakes on the subduction interface, we consider both a characteristic-type magnitude distribution near the upper magnitude limit and a Gutenberg and Richter-type distribution for earthquakes between **M** 7.5 and 8.5 (northern three zones) or **M** 9.0 (southern two zones). Earthquake rates are modeled using Gutenberg and Richter *b*-values, and magnitude distributions are described in the Data and Resources. The Papazachos *et al.* (2004) and

Table 2
Comparison of the **M** ≥ 7.5 Rates Considered in the Model and the Earthquake Rates since 1900

Zone	Model Rate (**M** ≥ 7.5)	Observed Rate ISC-GEM Catalog (**M** ≥ 7.5)
1	0.04	0.04/0.04
2	0.09	0.09/0.09
3	0.04	0.04/0.04
4	0.17	0.06/0.11 (0.14 since 1964)
5	0.05	0.04/0.04

ISC-GEM, International Seismological Centre-Global Earthquake Model.

Strasser *et al.* (2010) length–magnitude scaling relations for subduction interface earthquakes indicate maximum magnitudes from **M** 9.4 to 9.7 would be compatible with zone lengths. We base the earthquake rates on the subduction interface on historical earthquakes and allow for earthquakes with **M** 7.0–9.5 (±0.1) in the two southern zones, zones 4 and 5, and **M** 7.0–9.0 (±0.2) in the northern three zones (i.e., zones 1–3).

The rate of the characteristic ruptures in each zone is modeled as 400 yrs; this recurrence is based on several lines of evidence. First, it appears that the great 1960 Chile earthquake has similar effects as an earthquake in 1575 (Cisternas *et al.*, 2017); the time between these earthquakes is close to 400 yrs. Second, the 1960 Chile earthquake slipped several tens of meters and it would take about several hundred years to build up the seismic slip necessary to rupture in a subsequent event with the observed plate convergence rates (Barrientos and Ward, 1990). This model is consistent with observations and plate tectonic theory; however, future analyses should better define the 400-yr recurrence of these characteristic ruptures because this is a simple model which is only a first-order approximation of earthquakes and convergence rates along this complex zone.

The Gutenberg and Richter model is based on historic seismicity and on applying *b*-values of 0.8 or 0.9 to forecast the rate of larger earthquakes. A comparison of the **M** ≥ 7.5 rates considered in the model and the earthquake rates since 1900 is shown in Table 2. All of the model rates since 1900 are generally consistent with the observed rates except in zone 4 where the rates are more consistent with the earthquakes since 1964. Again, we suggest that future updates include a more extensive analysis of the magnitude–frequency distribution of these subduction interface earthquakes.

In addition to our model, we apply an alternative model for Chile developed by the Chilean experts that is described in Medina *et al.* (2017). We apply this model to zones 3–5, which includes Chile and Peru subduction interface models to account for additional epistemic uncertainty. We give equal weight to the Medina *et al.* (2017) source model and the USGS model (described earlier) derived in this analysis. In the USGS model, the zone 3 characteristic source has **M** 9.0 whereas in zones 4 and 5, the characteristic source has **M** 9.5, similar to the May 1960 **M** 9.5 Chile mainshock. The Medina *et al.* (2017) model also has two branches that consider tapered Gutenberg and Richter distributions. The taper begins at **M** 9.5, and M_{max} is 9.75 in these branches. The difference between the two branch models is that for the first model potential interface ruptures end at the Chile Rise, with latitude about 45° S. For the second model, ruptures may continue through the Chile Rise into the Antarctic plate, stopping at about 52° S. The weights that we assign to these two branches in this study are 0.4 and 0.1, respectively, to account for the half-weight assigned to the Medina *et al.* (2017) model. That is, they suggest a low probability that the Antarctic plate might participate in future subduction events in Chile based on historical rupture patterns.

The Medina *et al.* (2017) Gutenberg and Richter distribution parameters were determined from a seismicity catalog of earthquake hypocenters that includes sources with magnitudes ranging from **M** 4.5 to 9.5. Because the second model allows for ruptures that extend farther south, it is based on a larger seismicity catalog that includes sources in the Antarctic plate–South America plate interface region. The subduction sources, confined to the actual Nazca–South America plate interface, have M_{min} of 7.85 and M_{max} of 9.75, which is a little larger than the observed M_{max} in this region but consistent with the magnitude–area equations discussed earlier. The expected mean rate of earthquakes in this broad magnitude range is about 0.1013 for a mean recurrence interval of 9.87 yrs. Medina *et al.* (2017) discuss these models further, and they obtain a seismic plate convergence rate of about 55–75 mm/yr, depending on site location in Chile, which compares well with the geodetically determined plate convergence rate.

We also model additional subduction zones off the northern coast of South America that could influence sites within the continent: the Lesser Antilles subduction zone, two Panama deformation zones, and the northern coast subduction zone off the coastline of Colombia. Earthquakes along the Lesser Antilles subduction zone are modeled because they may affect the northernmost area of the South American continent. The northern portion of the Lesser Antilles zone seems to be more active and better defined than the southern part (Hayes *et al.*, 2014). For this model, we do not differentiate between earthquake rates in the north and south because earthquake rates on the southern Lesser Antilles zone are not well understood. We model simple characteristic earthquakes using a fault geometry based on Slab 1.0 (Hayes *et al.*, 2012) and with **M** 8.1 ± 0.3 with a recurrence of 400 yrs based on information provided by Hayes *et al.* (2014). The smoothed seismicity Gutenberg and Richter model layer extends up to **M** 7.8, so this model along with the characteristic model account for earthquakes up to **M** 8.5. The maximum historical magnitude is about **M** 8.25 (Hayes *et al.*, 2014).

The subduction zone along the northern coast of South America is not well defined by historical earthquakes. No large earthquakes with **M** ≥ 7 have occurred in this zone

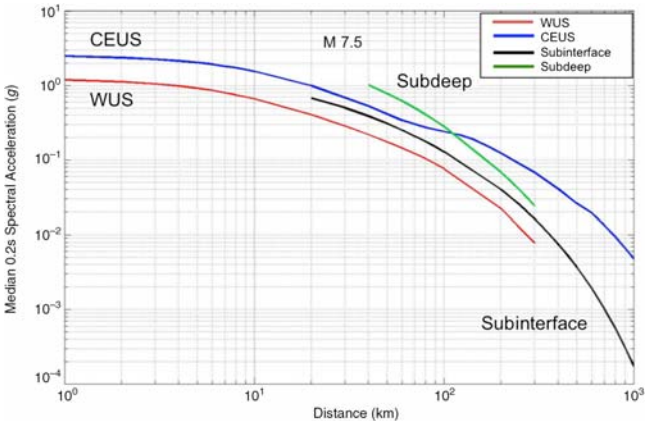

Figure 5. Average weighted ground-motion models used in the South America model and U.S. National Seismic Hazard Models (NSHMs) as a function of rupture distance for **M** 7.5 ground motions with site condition $V_{S30} = 760$ m/s for earthquakes in (1) stable continental regions or craton (central and eastern United States [CEUS]), active crustal faults (western United States [WUS]), subduction interfaces, and deep intraslab earthquakes. Curves for stable continental region apply distance conversions and extend out to 1000 km distance; shallow crustal earthquakes are strike-slip mechanism and extend to 300 km; subduction interface earthquakes are for 20 km depth in forearc regions and extend out to 1000 km; and deep intraslab earthquakes are located at 50 km depth and extend out to 300 km distance. The color version of this figure is available only in the electronic edition.

through the 500 yrs of recorded history and only sparse seismicity of lower magnitudes defines the zone (McCann, 2006). Nevertheless, McCann (2006) suggests that this zone poses an earthquake threat (with indeterminate potential) and Sykes *et al.* (1982) indicate that subduction processes have been ongoing since the late Eocene (38 Ma) in their plate tectonic reconstructions. Sykes *et al.* (1982) indicate subduction rates that are similar to those found in the Lesser Antilles subduction zone. Bird (2003) defines a North Andes plate and indicates complex tectonic interactions of several millimeters per year of relative motion involving the Panama plate, the Nazca plate, the South America plate, and the Caribbean plate. Slip rates from geodetic models such as that of Bird (2003) indicate similar values for this northern coast of South America and the Lesser Antilles subduction zones. Therefore, we model the subduction zone along the northern coast of South America using an analogy with rates defined in the Lesser Antilles subduction zone (0.5 weight). We also allow for a logic-tree branch that considers that this subduction zone is no longer capable of producing large earthquakes (0.5 weight) because few moderate and no large earthquakes have been observed along the zone in the past 500 yrs; if the modeled rates are reasonable, we probably would have observed more earthquakes during this period. The Panama deformation zones occur on both sides of the Isthmus of Panama. This region is outside South America but we modeled it based on previous work that was incorporated in the Panama building code to account for nearby sources (M. Petersen *et al.*, unpublished manuscript, 2005, see Data and Resources). Table 1 summarizes the source parameters for the subduction model.

We also consider the deep intraslab earthquakes in the model by smoothing the earthquake catalog locations horizontally at different depth intervals. The ISC-GEM catalog has fairly good depth control for earthquakes located at about 50 km because depth phases (*pP*) are often recognizable in the seismograms (Bondar *et al.*, 2015). We make separate gridded rate models for the seismicity at depths of less than 50 (shallow crustal), 50–100, 100–150, 150–200, and greater than 200 km. It would be difficult to associate a dipping zone that captures most of the data, unless the zone is very thick (i.e., several degrees in longitude). Therefore, smoothing the data into clouds at four depth ranges does a good job of capturing the essence of the hypocenter data. Some of the deep intraslab seismicity occurs under northeastern Colombia, suggesting active subduction. We compared the smoothed models with a modeled downgoing slab which shows some differences near Lima and many similarities. The model comparison maps, deep seismicity maps, probability of $\mathbf{M} > 5$ events, and input files are all available in the Data and Resources.

Table 3
Ground-Motion Model Parameters

Source	Ground-Motion Model (GMM)	Abbreviation	Weight
Active crustal regions	Abrahamson *et al.* (2014)	ASK13	0.22
	Boore *et al.* (2014)	BSSA13	0.22
	Campbell and Bozorgnia (2014)	CB13	0.22
	Chiou and Youngs (2014)	CY13	0.22
	Idriss (2014)	I13	0.12
Stable continental regions or craton	Atkinson (2008′)	A08′	0.08
	Atkinson and Boore (2006′)	AB06′	0.25
	Campbell (2003)	C03	0.13
	Frankel *et al.* (1996)	F96	0.06
	Pezeshk *et al.* (2011)	P11	0.17
	Silva *et al.* (2002)	S02	0.06
	Tavakoli and Pezeshk (2005)	TP05	0.13
	Toro *et al.* (1997), Toro (2002)	T02	0.12
Deep (intraslab)	Atkinson and Boore (2003) Cascadia Model	AB03Cascadia	0.1665
	Atkinson and Boore (2003) Global Model	AB03Global	0.1665
	BC Hydro (Abrahamson *et al.*, 2016)	BCHydro12	0.333
	Zhao *et al.* (2006)	Zhao06	0.334
Subduction (interface)	Atkinson and Macias (2009)	AM09	0.333
	BC Hydro (Abrahamson *et al.*, 2016)	BCHydro12	0.333
	Zhao *et al.* (2006)	Zhao06	0.334

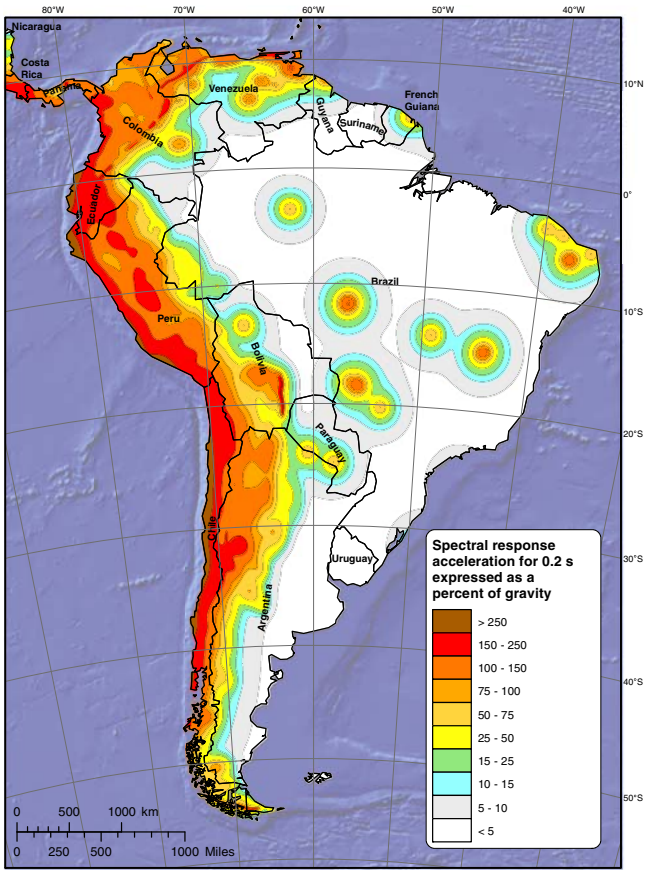

Figure 6. Seismic hazard for 0.2 s spectral acceleration (SA) for 2% probability in 50-yr hazard level on uniform rock (V_{S30} = 760 m/s). The color version of this figure is available only in the electronic edition.

Crustal Fault Model

The seismicity catalog developed for this hazard assessment (discussed previously in the Smoothed Seismicity Model section) accounts for about 200 yrs of recorded seismicity; however, we use only seismicity since 1964 in the smoothed seismicity model due to completeness constraints. We also recognize the need to account for earthquakes on faults that have not ruptured during this short period but have been active in the historic and prehistoric periods. Our crustal fault model accounts for such earthquakes.

In tectonically active regions across the globe, geomorphic and paleoseismic evidence of earthquakes has been studied and several hundreds of publications address these prehistoric events. A major effort to compile this information was conducted in the early 2000s for South America. The South America Quaternary fault and fold compilations (Costa *et al.*, 2000; Lavenu *et al.*, 2000; París *et al.*, 2000; Saadi *et al.*, 2002; Eguez *et al.*, 2003; Macharé *et al.*, 2003; Audemard *et al.*, 2005) reviewed by Costa *et al.* (2006) include information on hundreds of mapped Quaternary faults. However, few faults have been studied sufficiently for the scientific community to reach consensus regarding rate of deformation that can be applied in this hazard assessment. Costa *et al.* (2006) recognize that knowledge of Quaternary faults in South America remains incomplete.

We develop a crustal fault model that accounts for the fault geometry and rates of earthquakes. It is important to point out that our fault model is incomplete, overly simplistic, relies on scientific judgment, and samples only a short part of the geologic history. There are two essential pieces of information required for modeling faults: (1) the seismogenic source geometry and (2) the seismogenic source behavior (Haller and Basili, 2011). This information is derived from geological and geophysical studies of each fault. In our South America fault model, 2D fault geometry is generalized from digital fault traces compiled in the national Quaternary fault and fold compilations, and the depth of future ruptures and fault dips are typically not well understood. We assign default geometry for South American faults similar to those used in the USGS western United States (WUS) model (Petersen *et al.*, 2014, 2015). Many of the faults in the South America Quaternary fault and fold compilations are divided into sections. We model the full mapped length as an independent source hosting floating ruptures (incomplete ruptures that fill the fault source) with a maximum magnitude up to **M** 7.5 for dipping faults and **M** 8 for strike-slip faults. Additional floating ruptures include magnitudes of **M** 6.5 to the maximum magnitude for the specific source.

One important modeling parameter is the rate of earthquake activity, which is typically constrained by mean slip rate as a function of rake and dip. Generally geologic studies report vertical- or horizontal-displacement rate as slip rate but give no consideration to displacement on the fault plane. Rates of deformation have been shown to fluctuate both in space and time, making it difficult to assess the activity rate in seismic hazard assessments and increasing uncertainties. Uncertainties in these fault inputs are large due to inaccuracy in distinguishing the timing and locations of past ruptures, variability in along-strike slip in a single rupture or suite of ruptures, and inaccuracy in dates of prior earthquakes. Therefore, the quality of slip rate varies, and almost always, the knowledge of a given fault-slip rate is limited by too few site investigations and the limited length of the geologic record.

For some faults, we model earthquakes across a zone that is constrained by geologic or geodetic data. For example, geodetic data suggest the Quito fault in Ecuador is deforming at high rates (Alvarado *et al.*, 2014); however, little geologic evidence exists that corroborates such high rates. Some of the deformation may be accommodated on faults that are not well expressed at the surface. Thus, we model two compressional zones; the small zone is constrained to the lateral extent of the Quito fault and the large zone spans the gap between the Pallatanga and Chingual faults and represents the continuous zone of compressional faults along the western foothills of the Andes. High rates of slip on the Bocono fault to the west and the combined rate of the

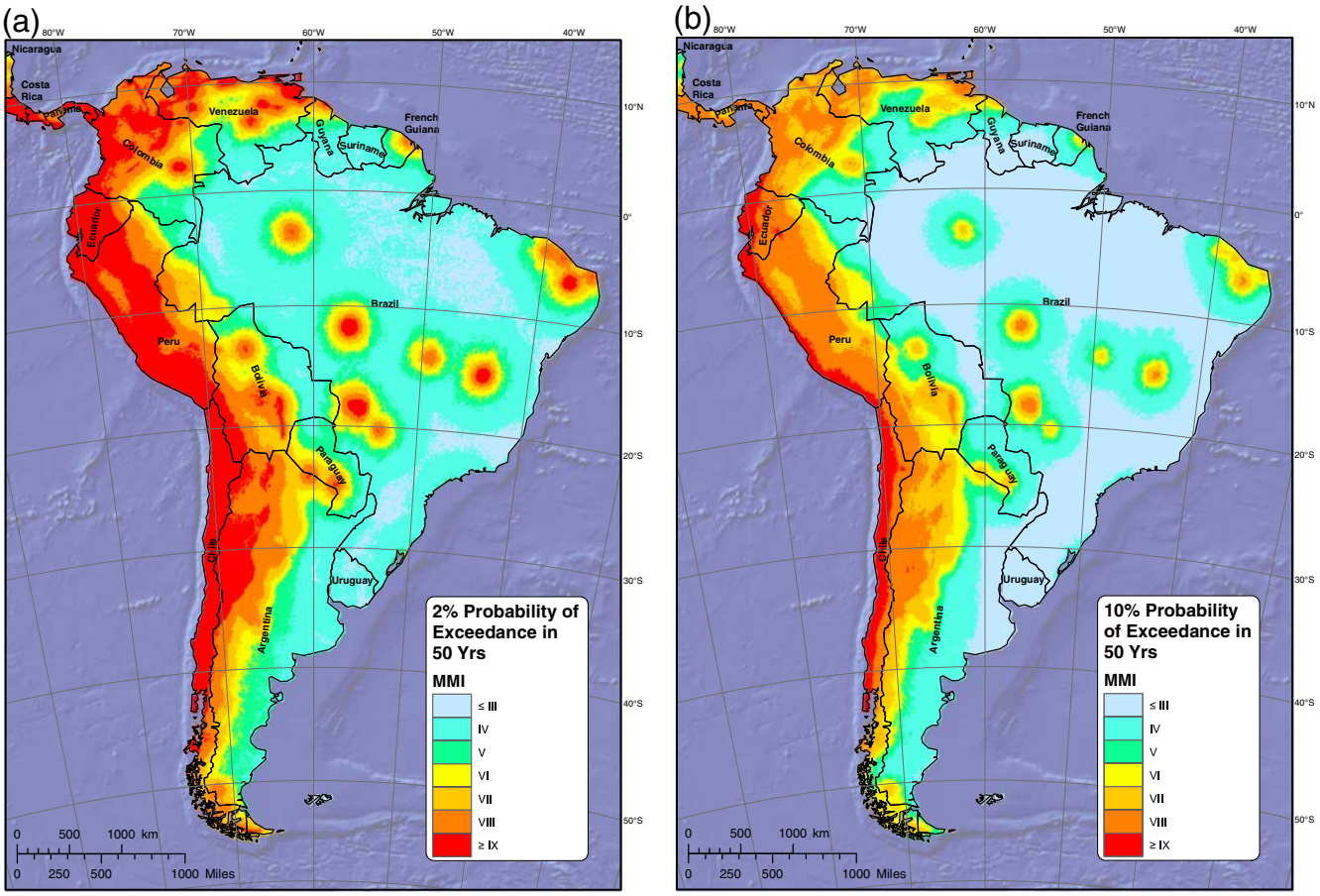

Figure 7. Modified Mercalli intensity (MMI) probability of exceedance hazard maps for (a) 2% in 50 yrs, (b) 10% in 50 yrs, and (c) 50% in 50 yrs. The color version of this figure is available only in the electronic edition. (*Continued*)

San Sebastian and the El Pilar fault suggest that some of the regional deformation is accommodated by faults south of the San Sebastian fault. The Valencia source zone was introduced to accommodate the remaining 5 mm/yr of shearing.

Our South America crustal fault model includes fewer fault sources than our earlier hazard; the 2010 USGS model contained more than 100 faults, most of which were slowly deforming and did not contribute much to total hazard. In the prior assessment, faults were assigned displacement rates defined by the slip rate category in the South America Quaternary fault and fold compilations, which results in rates that are not reliable. Nevertheless, by the end of the 2000s the activity rates for 26 faults in South America were constrained by published science and were applied in our current crustal fault model (Fig. 3 shows geometry for each of these faults). The selection criteria used in this model include faults with annual earthquake rates of 1 in 2475 or greater and **M** 6.8 or greater. This excludes faults that have low activity rates, small rupture sizes, or that are poorly studied, and so these are modeled using the smoothed (gridded) seismicity model. Figure 3 shows the fault sources and Table 1 summarizes the source parameters of the crustal fault model.

Ground-Motion Model

In developing our hazard model for South America, we considered GMMs that were applied in the USGS NSHMs (Rezaeian *et al.*, 2015). We consider the United States models because almost all of these equations consider global earthquakes and because the United States and South America are seismically quite similar with potential for active subduction, deep intraslab, crustal, and craton earthquakes (Petersen *et al.*, 2014, 2015). Figure 5 shows the mean of the weighted GMMs applied in the U.S. NSHMs. Table 3 summarizes the GMMs selected and weights applied for our ground-motion model for South America. Active crustal earthquakes are modeled using five alternative GMMs from the Next Generation Attenuation (NGA)-West2 project; earthquakes in the stable continental region or craton are modeled using eight GMMs; subduction interface earthquakes are modeled using three GMMs; and deep gridded seismicity is modeled using four GMMs. Weights applied to the GMMs are the same as those developed for the USGS NSHMs. These equations are based on global data as well as simulated data and the weights are applied by comparing the models with recent strong-motion data and by excluding

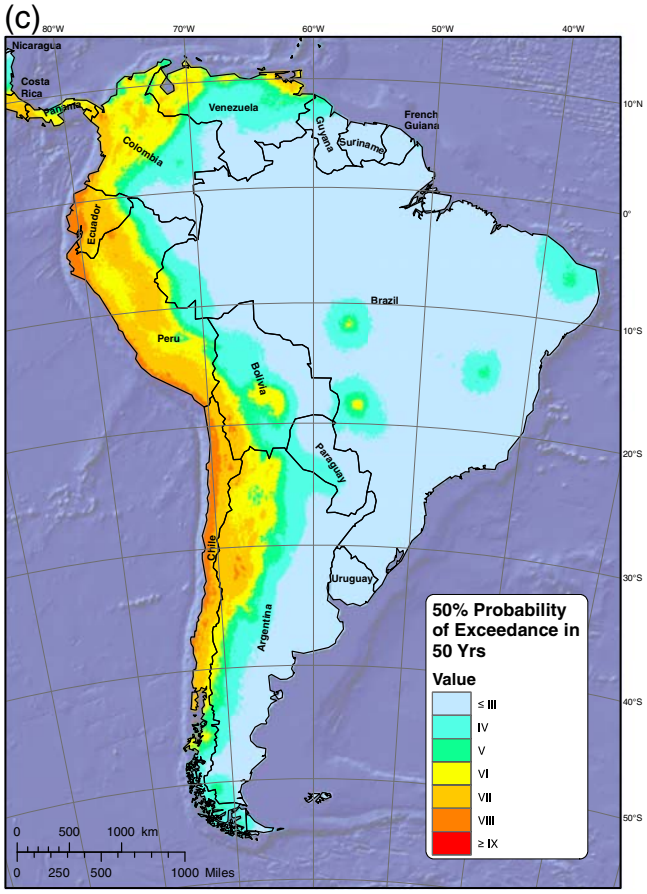

Figure 7. Continued.

models that do not provide the necessary outputs needed for calculating the hazard.

Figure 5 shows the median 0.2 s (5 Hz) SA as a function of rupture distance for an **M** 7.5 earthquake and for the four classes of GMMs used in the hazard calculations. The central and eastern United States (CEUS) model is for stable continental regions or cratons and yields the highest ground motion out to about 40 km distance. The subduction deep model characterizes intraslab or deep earthquakes and gives the highest motions for distances from 40 to 100 km. The subduction interface model produces lower values than the craton or intraslab earthquakes but is a major contributor to ground motion at large distances (especially for longer periods such as 1 s spectral SA). The WUS curve is for shallow crustal earthquakes and is lower than the others but contributes significantly to strong ground shaking at close distances.

Results

Seismic hazard maps were produced for 2%, 10%, and 50% probability of exceedance in a 50-yr period, for various ground-motion parameters (e.g., PGA, MMI, or SA with 5% damping for various periods) and for a uniform site condition of V_{S30} of 760 m/s (firm rock, or with amplifications considered). The seismic hazard map for 0.2 s (5 Hz) SA with a 2% probability of exceedance in 50 yrs is presented in Figure 6. High hazard is calculated along the western and northern coasts of the continent but other areas are also highlighted, with higher hazard in places where past large earthquakes have occurred. A small region in central Colombia is thought to be caused by induced or man-made earthquakes, so these places should be reanalyzed in future studies. Ground-motion hazard is greater than 1*g* at multiple sites along the western coast of the continent. The 2010 USGS model considered many more slow-slip-rate faults that did not contribute as much to hazard (comparisons of this model and the 2010 model can be found in Data and Resources).

Figure 7 shows the MMI maps for 2%, 10%, and 50% probability of exceedance in 50 yrs that are consistent with rare, possible, and likely ground-shaking levels, respectively. These MMI maps were derived from PGA hazard conversions of Worden *et al.* (2012), amplification based on a topographic proxy of Allen and Wald (2009), and site amplifications based on Seyhan and Stewart (2014) relationships. These conversion and amplification relationships were developed mostly from seismic data in active continental regions and not cratonic regions, but very few equations are available that discuss regional differences. Worden *et al.* (2012) show that the intensities in the CEUS may be higher for a given PGA than in the WUS, especially for intensities less than MMI V. New regional amplification models are currently being considered for the CEUS but as yet we do not include any of these models in the United States hazard and building design models. Future studies should re-examine these relationships to account for regional crustal differences. There could be additional uncertainties in such conversions; refer to Silva *et al.* (2014) for further discussion on this topic. MMI greater than VI represents damaging ground-shaking levels and is consistent with about 0.12*g* PGA and 0.1*g* 1 s SA (Worden *et al.*, 2012). Therefore, much of the western and northern coasts of South America have a significant chance for damaging ground shaking in the next 50 yrs.

We compared the new 2017 USGS model with the 2010 USGS and the GSHAP (1999) models to see how the new model differs from previous models (Petersen *et al.*, 2017). All of the comparisons were made as ratios of PGA at 10% probability of exceedance in 50 yrs. We do not include the ratio maps in this article but include them in supplementary material available at ScienceBase (see Data and Resources). Ratio maps of the 2017 USGS and the 2010 USGS models indicate that tectonically active parts of South America along the west and north coast are in reasonable agreement, differing by less than 20% almost everywhere. Larger differences are observed east of the Andean cordillera, where the hazard is higher near locations of several earthquakes that were reanalyzed in the GEM-ISC catalog, but lower at places such as eastern Argentina, where earthquake rates were modified due to changes in catalog completeness assumptions. We recognize that these areas should be reexamined by local

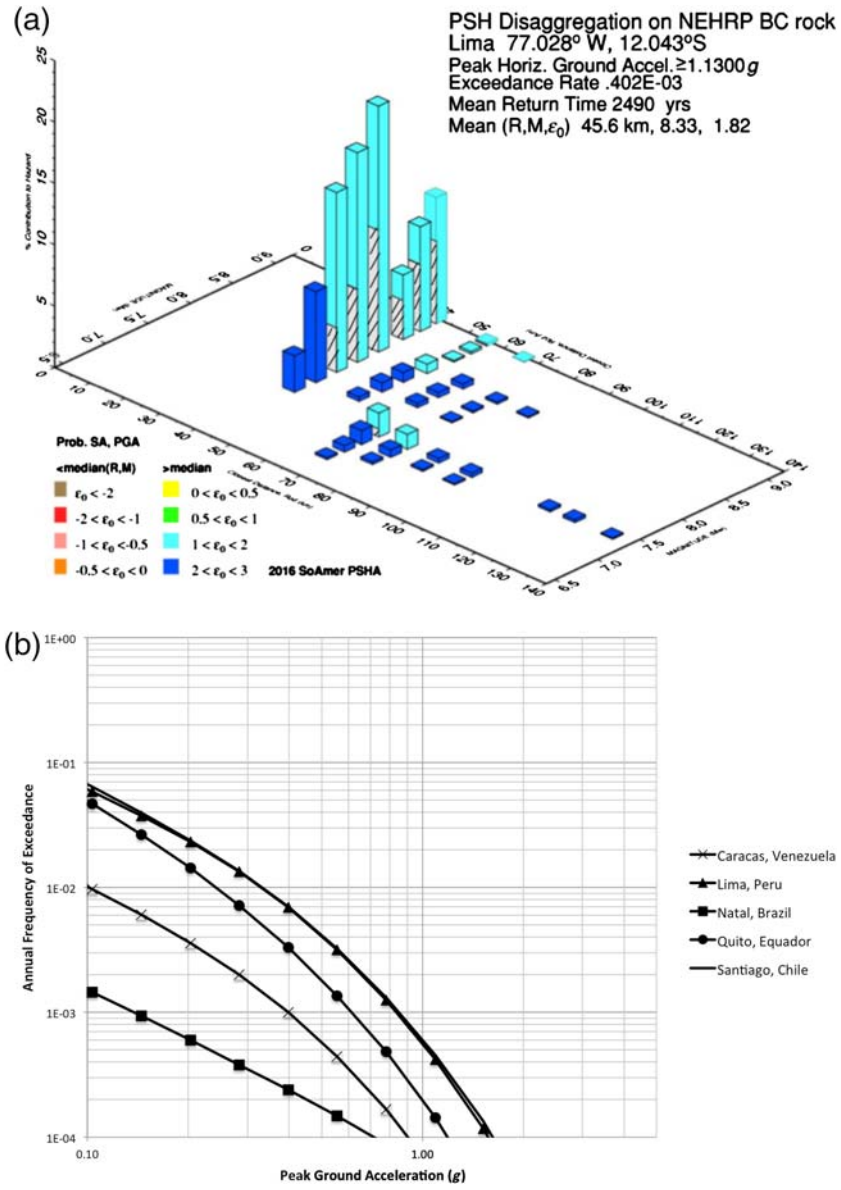

Figure 8. (a) Deaggregation of Lima, Peru, and (b) peak ground acceleration (PGA) total mean hazard curves for five sites across South America. The bars in (a) are shaded according to the epsilon bin for which the contribution to hazard is greatest. The hatched bars represent the contributions for lower epsilon bins. The color version of this figure is available only in the electronic edition.

seismologists for implementation in country-based maps. Several fault sources were omitted from the new model because the recurrence information was not well constrained. Again, local experts should assess fault input maps used in public policy hazard and design maps. Ratio maps of the 2017 USGS and GSHAP (1999) models show some larger differences. The 2017 USGS model predicts higher PGA along the tectonically active regions because GSHAP (1999) did not include explicit subduction and crustal fault sources in these areas. In the area east of the cordillera, the results are mixed and dependent on the earthquake locations, magnitudes, earthquake source models, and GMMs.

Deaggregation plots and hazard curves were produced for multiple sites in South America. An example deaggregation plot for Lima, Peru, that shows the relative contribution of individual sources to the seismic hazard (aggregated by magnitude and distance) is shown in Figure 8a. This plot shows that large magnitude subduction interface sources are dominating hazard at this site. Peru has experienced damage from such earthquakes throughout its history. PGA total mean hazard curves for multiple sites in South America are shown in Figure 8b. Sites on the western side of South America, located along the subduction zone, show the highest levels of hazard. Additional seismic hazard maps, source model information, and deaggregation plots may be obtained at ScienceBase (see Data and Resources).

PAGER Risk Assessment

In this section, we investigate the potential impact of our probabilistic earthquake hazard analysis on human and built environments in South America. For this, we rely on the USGS PAGER datasets and tools for performing exposure and loss/risk analyses as discussed below (Wald *et al.*, 2008). These risk estimates are simple models and do not yield exact losses; they are highly uncertain. Nevertheless, these values may be useful for comparing relative potential losses across the continent.

Exposure Analysis

For exposure analyses, we make use of gridded population data (geospatial resolution of ~30 arcsec; that is, roughly 1 km × 1 km grid cell) available through LandScan 2012, developed by the Oak Ridge National Laboratory team (Bhaduri *et al.*, 2002). We overlaid the gridded population data on earthquake frequency and MMI probabilistic hazards maps (Fig. 7) and performed spatial analyses to compare the human exposure with different levels of shaking intensity.

More than one-third of the total population in South America, or about 160 million people out of 400 million total people, may experience strong ground shaking from earthquakes in a 50-yr period (2% probability of exceedance in 50 yrs). These population numbers are similar but slightly larger than those determined in a similar study that assessed

Table 4
Population Exposure across South America and Adjacent Countries

Probability			Estimated Population Exposed to MMI		
Estimated Population Exposed to MMI	Country	Population (2012)	≥ VI	≥ VII	≥ VIII
50% probability of exceedance in 50 yrs	Argentina	42,252,339	7,289,971	2,852,338	65,544
	Bolivia	10,226,808	5,343,868	145,119	1,069
	Brazil	199,378,759	57,618	94	
	Chile	17,061,842	16,812,386	16,680,552	10,466,603
	Colombia	45,166,135	41,670,074	10,062,139	172,599
	Ecuador	15,210,601	15,181,638	14,863,094	7,373,660
	French Guiana	230,132			
	Guyana	743,163			
	Panama	3,494,547	3,255,892	569,105	2,072
	Paraguay	6,517,827			
	Peru	29,529,602	28,600,391	23,959,455	14,982,434
	Suriname	558,878			
	Trinidad and Tobago	1,226,382	1,226,382	893,797	
	Uruguay	3,324,541			
	Venezuela	28,092,185	19,336,605	1,451,377	1,214
	Total	403,013,741	138,774,825	71,477,070	33,065,195
10% probability of exceedance in 50 yrs	Argentina	42,252,339	11,373,023	9,075,745	5,833,576
	Bolivia	10,226,808	9,321,545	7,793,742	2,661,626
	Brazil	199,378,759	11,270,310	2,181,824	201,225
	Chile	17,061,842	17,047,034	16,887,235	16,799,531
	Colombia	45,166,135	44,870,129	44,544,329	25,051,809
	Ecuador	15,210,601	15,209,489	15,193,262	15,063,892
	French Guiana	230,132	143,804	62,506	
	Guyana	743,163	54,987	15,659	
	Panama	3,494,547	3,494,547	3,487,064	2,868,379
	Paraguay	6,517,827	1,993,559	15,119	
	Peru	29,529,602	28,859,386	28,758,449	27,169,495
	Suriname	558,878			
	Trinidad and Tobago	1,226,382	1,226,382	1,226,382	1,158,829
	Uruguay	3,324,541			
	Venezuela	28,092,185	27,035,859	25,759,371	14,220,917
	Total	403,013,741	171,900,054	155,000,687	111,029,279
2% probability of exceedance in 50 yrs	Argentina	42,252,339	13,397,276	11,712,780	10,538,330
	Bolivia	10,226,808	9,761,987	9,382,045	8,130,269
	Brazil	199,378,759	20,604,743	13,346,338	9,093,847
	Chile	17,061,842	17,056,835	17,051,949	16,909,051
	Colombia	45,166,135	45,038,363	44,937,357	44,657,728
	Ecuador	15,210,601	15,210,601	15,209,925	15,192,476
	French Guiana	230,132	154,858	148,102	120,216
	Guyana	743,163	487,081	71,348	27,450
	Panama	3,494,547	3,494,547	3,494,547	3,492,394
	Paraguay	6,517,827	3,557,996	2,705,533	1,513,710
	Peru	29,529,602	29,466,483	29,385,432	28,832,342
	Suriname	558,878			
	Trinidad and Tobago	1,226,382	1,226,382	1,226,382	1,226,382
	Uruguay	3,324,541			
	Venezuela	28,092,185	27,893,723	27,079,324	26,161,927
	Total	403,013,741	187,350,875	175,751,062	165,896,122

MMI, modified Mercalli intensity.

vulnerable populations using the Global Seismic Hazard Map (Jaiswal *et al.*, 2014). About 110 million people live in areas where earthquakes are more likely (10% in 50 yrs), and 30 million reside in areas of high hazard where earthquake are quite likely (50% in 50 yrs). Countries such as Bolivia, Chile, Ecuador, Peru, and Venezuela have large populations that may be vulnerable to strong shaking. Table 4 shows the vulnerable populations counts by country for South America, Panama, and Trinidad and Tobago with alternative hazard levels.

Risk Analysis

We also calculate the seismic risk, which is expressed in terms of average annual loss (AAL) per country, using PAG-

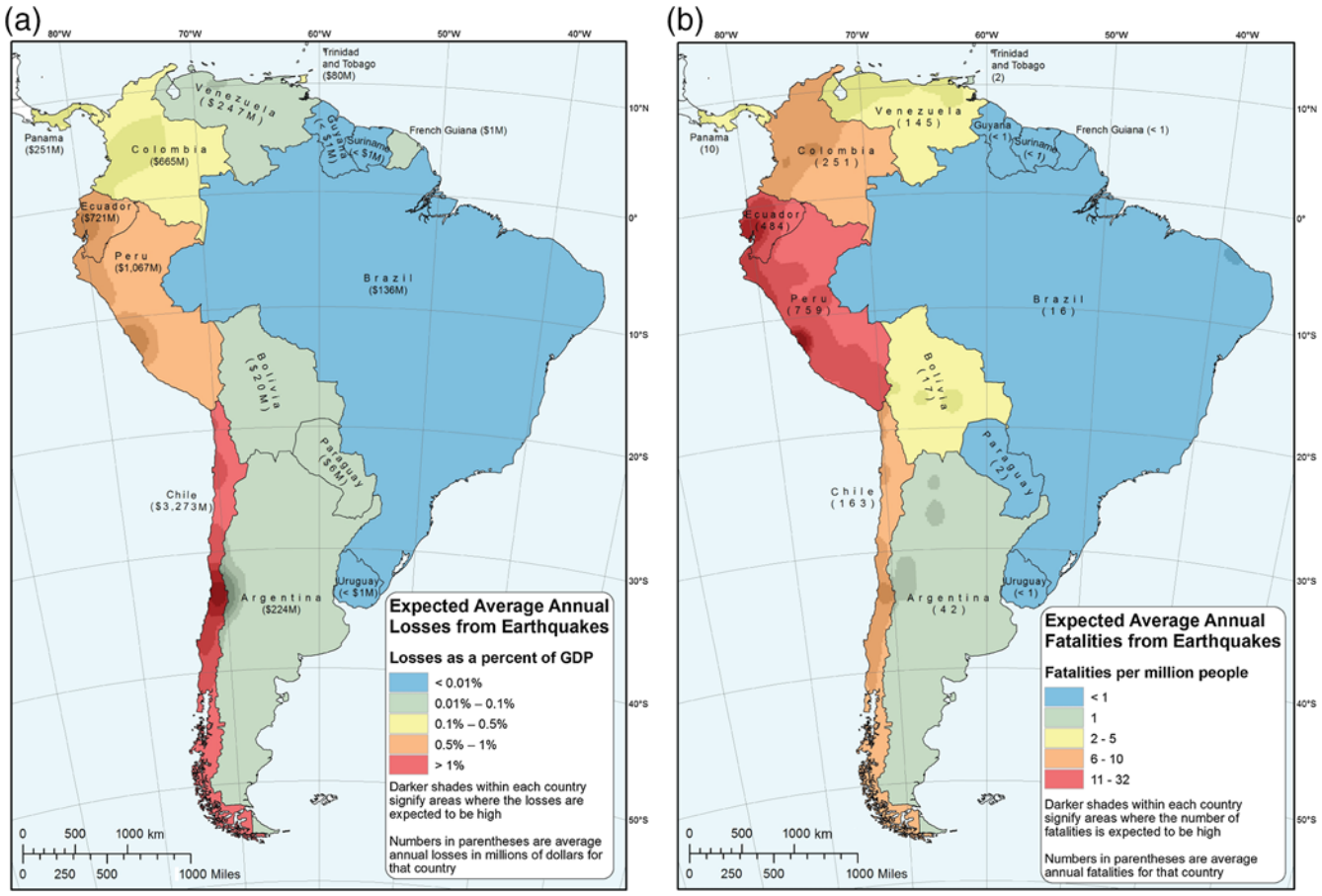

Figure 9. Prompt Assessment of Global Earthquakes for Response (PAGER) risk maps for MMI. Shadings represent losses as a percent of gross domestic product (GDP); (a) expected average annual losses from earthquakes and (b) expected average annual fatalities. The color version of this figure is available only in the electronic edition.

ER's empirical vulnerability relationships developed by Jaiswal and Wald (2010, 2011). In this study, the authors used the comprehensive seismicity catalog of all significant worldwide earthquakes (**M** 5.5 and above) since 1973 and derived country-specific empirical vulnerability relationships to estimate earthquake shaking-induced fatalities and direct shaking-related economic losses. To parameterize earthquake fatality and economic loss ratios as a function of MMI, we assumed a two-parameter cumulative lognormal distribution. The procedure led to development of unique vulnerability functions for each country or group of countries where four or more fatal earthquakes have occurred during the last 35+ yrs. In the calibration process, all earthquakes (i.e., damaging as well as nondamaging) were included. For countries where empirical data were lacking, we proposed a globally consistent regionalization scheme based on a number of socioeconomic indicators to relate countries that share similar vulnerability traits. The empirical relationship for fatality estimation for Peru indicates a rate of 1 death per 245 people exposed to shaking intensity IX and 1 death per 7604 people exposed to intensity VII. Similarly, for Chile, the PAGER model indicates a rate of 1 death per 833 people exposed to shaking intensity IX and 1 death per 32,082 people exposed to intensity VII. As we can note, there are significant differences in fatality rates at different intensities between different countries, which are indicative of their relative vulnerability to earthquakes. Readers are referred to the USGS website to access the information (see Data and Resources).

These relationships are highly approximate (an order of magnitude accuracy in general for places that lack empirical loss data), broader (mainly country-specific), empirically driven (only indirectly account for change in building code, construction practices), and a proxy approach to quantifying aggregated earthquake losses. The procedure bypasses the requirement of the detailed building-type-specific inventory and exposure and vulnerability/fragility data to perform loss/risk assessment for each geographic region such as those described in the Federal Emergency Management Agency (FEMA) Hazus-MH 2.1 Technical Manual (see Data and Resources) and Jaiswal *et al.* (2015).

The mean value of loss at each level of shaking intensity is estimated using the human and economic exposure and Jaiswal and Wald (2010, 2011) vulnerability models. Then, we integrated the losses for a range of intensities and their expected frequencies over the full hazard curve to estimate the AALs expected for each grid cell. Given the varying levels

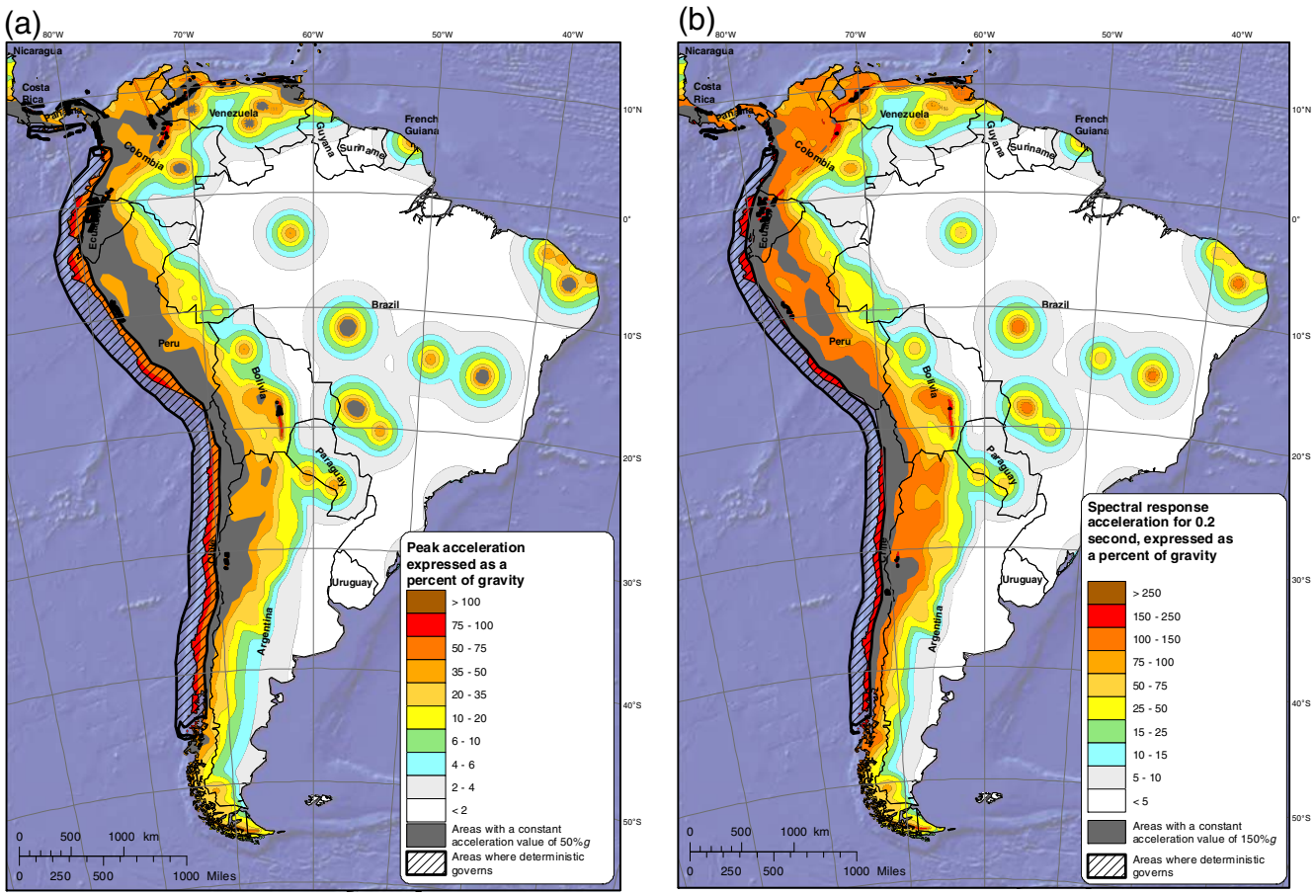

Figure 10. Seismic design maps for (a) peak acceleration, (b) 0.2 s SA, and (c) 1 s SA. The color version of this figure is available only in the electronic edition. (*Continued*)

of earthquake hazard and human and economic exposure in South America, the AALs measured in terms of deaths and dollar values for each country are represented in terms of per capita loss ratio as shown in Figure 9. As shown in Figure 9, given the very high earthquake hazard and high vulnerability of their built infrastructure to earthquake shaking, both Peru and Ecuador have the highest earthquake risk in terms of mortality (with highest average annual estimated fatality risk per million people exposed to earthquakes). Both Chile and Colombia are also situated very close to the highly active subduction zone and face high earthquake hazard, but these countries have lower vulnerability compared with Peru and Ecuador and thus have lower mortality risk. Figure 9 also highlights the areas within each country where the mortality or monetary risk is expected to be higher compared with other parts within that country (shown in darker shades). Contrary to the mortality risk, the monetary risk (expressed in terms of annualized direct economic losses due to shaking) is highest in Chile (~$3.3 billion U.S. per year), with one of the highest per capita gross domestic products (GDP) in South America and the largest in terms of per capita economic exposure subjected to strong shaking. At first glance, the estimated annualized losses for Chile may appear to be very high given its small geographic area in the subcontinent, but note that the recent **M** 8.8 Maule earthquake in Chile that occurred in February 2010 caused an enormous economic impact, estimated by Chile's government at approximately $30 billion U.S. (~15% of GDP), with the greatest part (about 21 billion) due to the destruction of infrastructure (with 370,000 houses, roughly 10% of total housing stock, damaged or destroyed; see Data and Resources). Countries such as Peru, Ecuador, and Colombia also experience high annualized earthquake shaking related losses of ~1 billion, ~720 million, and ~665 million per year, respectively, as shown in Figure 9. The annualized losses discussed here are highly approximate and are indicative of a long-term averaged value of direct shaking-related economic losses from all earthquakes that are expected to occur in a given country; earthquake losses from any individual earthquake could easily exceed this value.

The risk analyses quickly help to identify the areas of low and high relative seismic risks both in terms of mortality and monetary risk over the entire subcontinent. It is important to keep in mind that the uncertainties on these risk values are large (more than a factor of two) and that it is most useful to view these numbers relative to other regions rather than rely on the absolute numbers.

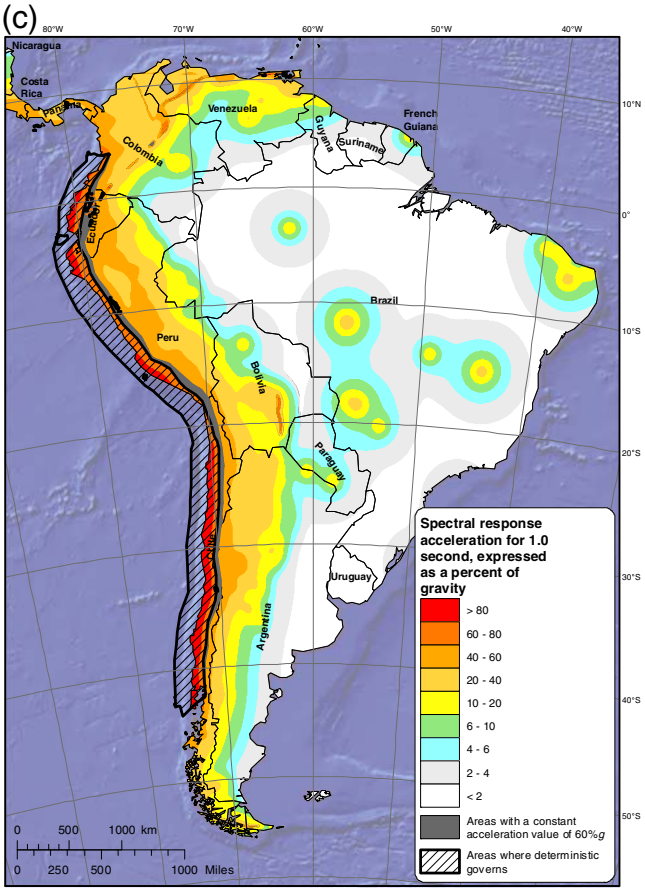

Figure 10. Continued.

Seismic Design Maps Compatible with the International Building Code

Based on the USGS NSHMs for the United States and its territories, and with funding from FEMA, the BSSC Provisions Update Committee (PUC) has developed earthquake ground-motion design maps that have been adopted by U.S. building codes. Following the same procedures (described below), we prepare analogous design maps for South America based on the hazard model described in the Seismic Hazard Model section. These design maps could be used for situations in which U.S. building codes are applied in South America (e.g., U.S. Department of Defense, 2016), or for comparisons with maps in South American building codes.

The BSSC PUC has developed two main sets of design maps for the United States and its territories: (1) risk-targeted MCE_R spectral response acceleration maps at vibration periods of 0.2 and 1.0 s and (2) maximum considered earthquake geometric mean (MCE_G) PGA maps. The MCE_R ground-motion maps are for the design of buildings and other structures, and the MCE_G ground-motion maps are for assessment of the potential for liquefaction and soil strength loss, as well as for determination of lateral earth pressures in the design of basement and retaining walls. Both types of maps are derived from the USGS NSHMs in accordance with the site-specific ground-motion procedures (sections 21.2 and 21.5 for MCE_R and MCE_G, respectively) of the NEHRP Recommended Seismic Provisions for New Building and Other Structures (BSSC, 2015) and the ASCE Minimum Design Loads for Buildings and Other Structures (also known as the ASCE 7 Standard; ASCE, 2016). The MCE_R and MCE_G ground motions are each taken as the lesser of probabilistic and deterministic values, as explained below.

The probabilistic MCE_R and MCE_G ground motions are derived from hazard curves such as those illustrated in Figure 8b. The probabilistic MCE_R spectral response accelerations are determined via iterative integration with a collapse fragility curve that is a function of the risk-targeted ground motions themselves, as stipulated in section 21.2.1.2 of ASCE 7-16 and detailed in Luco *et al.* (2007). As such, the risk-targeted ground motions take into account differences in the shapes of hazard curves. When used in design, risk-targeted ground motions are expected to result in buildings with geographically uniform mean annual frequency of collapse (1% probability of collapse in 50 yrs). Prior to the iterative integration, the hazard curves—which are for ground-motion parameters akin to the geometric mean of two horizontal components (e.g., the RotD50 average horizontal component from Boore, 2010, used by NGA-West2)—are converted to represent the maximum spectral response acceleration in the horizontal plane. The conversion is done via the scale factors specified in section 21.2 of ASCE 7-16, namely 1.1 and 1.3 for the 0.2 and 1.0 s spectral response accelerations, respectively. In contrast, the probabilistic MCE_G PGAs are simply interpolated from the geometric mean hazard curves at a mean annual frequency of 1 in 2475, corresponding to a 2% probability of exceedance in 50 yrs.

The deterministic values are taken to be the mapped MCE_R and MCE_G ground motions wherever they are less than their probabilistic counterparts (described above) and are computed from the models of earthquake sources and ground-motion propagation that underlie the USGS NSHMs. As defined in sections 21.2.2 and 21.5.2, respectively, the deterministic MCE_R and MCE_G values are each taken as the largest 84th-percentile ground motion for "characteristic earthquakes on all known active faults within the site region," (ASCE, 2016; p. 206) with the following lower limits for the maps: 1.5g and 0.6g for the 0.2 and 1.0 s deterministic spectral response accelerations, respectively, and 0.5g for the deterministic PGAs. These deterministic lower limits mean that the mapped MCE_R and MCE_G ground motions are probabilistic wherever they are less than the limits (i.e., 1.5g, 0.6g, or 0.5g). As explained in the commentary of ASCE 7-16, the 84th-percentile ground motions for the MCE_R and MCE_G maps are approximated as 1.8 times median ground motions from each characteristic earthquake. As with the probabilistic MCE_R spectral response accelerations described in the preceding paragraph, the deterministic MCE_R values are also converted to maximum-response ground motions, using the same scale factors (i.e., 1.1 and 1.3 for 0.2 and 1.0 s spectral response accelerations, respectively).

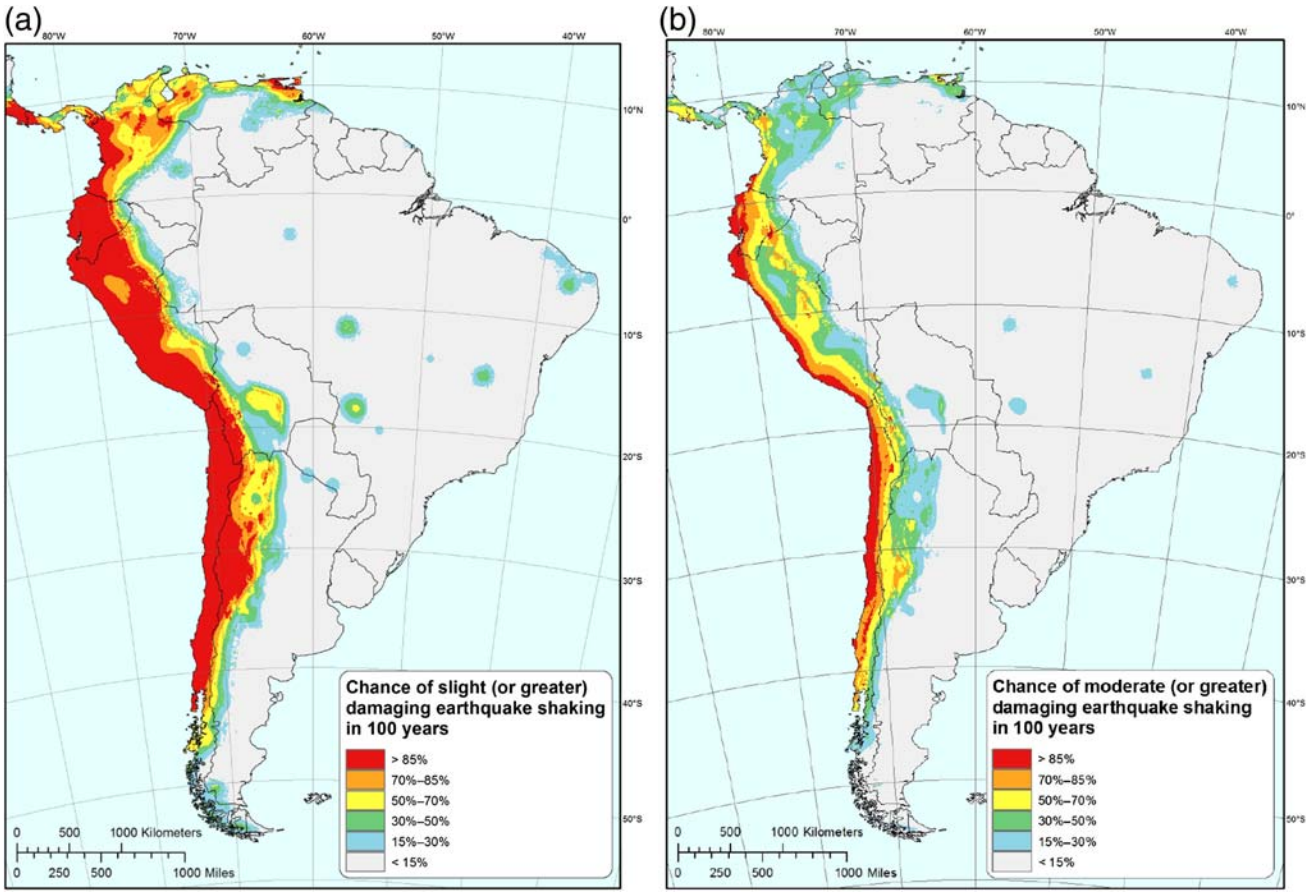

Figure 11. Chance of (a) slight (MMI ≥ VI), (b) moderate (MMI ≥ VII), or (c) considerable (MMI ≥ VIII) damaging earthquake shaking in 100 yrs. The color version of this figure is available only in the electronic edition. (*Continued*)

Based on the USGS hazard model for South America and the ASCE 7-16 procedures described above, Figure 10 provides MCE_R and MCE_G ground-motion design maps for South America, respectively. Because the International Building Code (IBC; International Code Council, 2015) has adopted such maps for the United States and its territories, the design maps for South America allow structural engineers to apply the IBC there. The design maps we prepared can also be compared with the maps mandated in the national building codes of South America.

Conclusions

In this article, we use the data, models, and methods of the USGS NSHMs to produce South American seismic hazard, exposure, risk, and design assessments that can provide additional information to public policy makers in developing risk mitigation strategies. In addition, these data may be helpful input for scientists and engineers developing new country-specific hazard and design maps or for comparison with current models. We do not recommend that these models be used directly in building codes or other public policy. Region-specific hazard models and maps as well as design standards should be provided by local experts, who can provide more detailed information, guide future hazard research, and contribute to the process of implementing the data into design procedures. Nevertheless, these regional models can be useful comparisons of the hazard, risk, and losses across the continent.

In this article, we updated our 2010 USGS model using a new seismicity catalog, fault data, subduction zone information, and ground-motion models. Comparison of this updated model with the publicly available GSHAP (1999) and 2010 USGS model indicates that much of the western coast of South America faces higher seismic hazard than previously recognized, but the ground shaking decreases more rapidly with distance than in the previous models. These higher coastal hazards are located in Venezuela, Colombia, Ecuador, Peru, and Chile; western Argentina and Bolivia also have relatively high hazard. This model also incorporates the observed seismicity in the inland regions of Brazil, Paraguay, Bolivia, and parts of Colombia causing higher hazard near past events and incorporates a better suite of crustal faults and activity rates that help refine the hazard.

More than 160 million people (or about a third of people living in South America) reside in areas that may be subjected to strong ground shaking. Figure 11 shows the spatial potential for damaging ground shaking quantified as slight

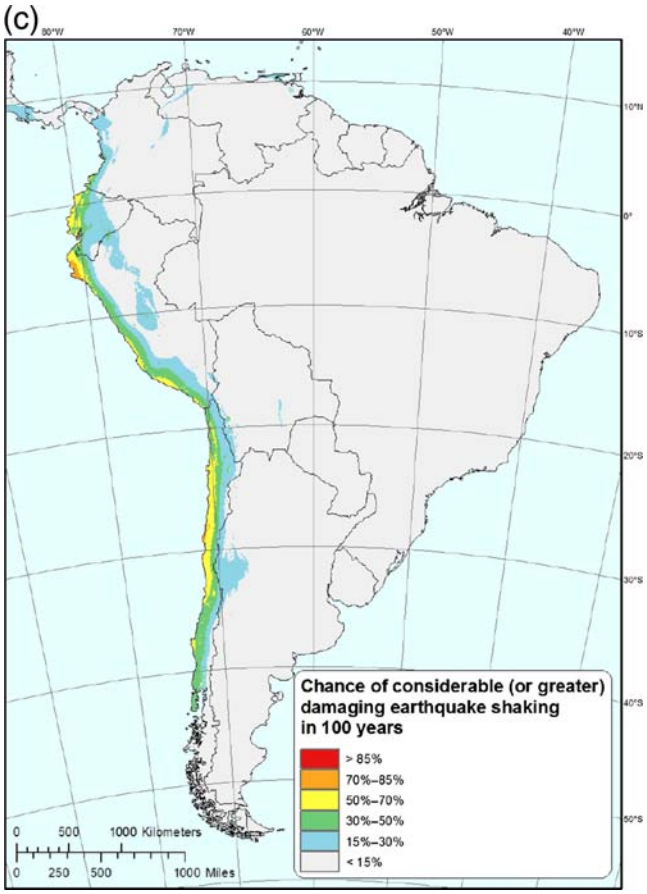

Figure 11. Continued.

(MMI > VI), moderate (MMI > VII), and considerable (MMI > VIII) during a century. These maps illustrate the highest potential along the west coast where large damaging earthquakes occur about every decade or so. Hazard is also significant on the northern coast of South America. This analysis helps to highlight that seismic hazard and risk occurs across many portions of South America, and is not limited to coastal areas. In particular, countries such as Venezuela, Colombia, Ecuador, and Peru face high hazard and seismic risk; Chile also faces high hazard, but the vulnerability of the built stock is lower compared with the northern countries. Our analysis highlights the need for rigorous country-specific efforts that include local experts to better quantify the hazard and mitigate these risks. National level efforts would be helpful in refining the continental scale seismic hazard assessment presented here. All of the datasets and models proposed here are publicly available at ScienceBase (see Data and Resources).

Data and Resources

The 2010 U.S. Geological Survey (USGS) model for South America can be found at https://earthquake.usgs.gov/hazards/images/SAmer-Proceedings2010.pdf (last accessed November 2017). Seismicity data were obtained from the International Seismological Centre Global Earthquake Model (ISC-GEM) Global Instrumental Earthquake Catalogue at http://www.isc.ac.uk/iscgem/request_catalogue.php (last accessed November 2017) through 2013 and supplemented since 2013 with seismicity data from the Advanced National Seismic System (ANSS) Comprehensive Earthquake Catalog (ComCat) at http://earthquake.usgs.gov/earthquakes/search/ (last accessed November 2017). The Regional Center for Seismology for South America (CERESIS) historical maximum intensity map for a 460-yr period from 1520 to 1981 can be found at http://www.ceresis.org/ (last accessed November 2017). The South America Risk Assessment (SARA) project information is available at https://sara.openquake.org/ (last accessed November 2017). Data for the Panama region comes from a 25 page unpublished 2005 manuscript submitted to the Panama Canal Authority titled Preliminary update of the probabilistic seismic hazard analysis for sites along the Panama Canal zone by M. Petersen, E. Schweig, C. Mueller, S. Harmsen, and A. Frankel. Prompt Assessment of Global Earthquakes for Response's (PAGER) empirical vulnerability relationships can be found at http://pubs.usgs.gov/of/2009/1136/ (spreadsheet for fatality models and spreadsheet for economic loss ratio models) (last accessed November 2017). Federal Emergency Management Agency's (FEMA) Hazus-MH 2.1 Technical Manual can be found at https://www.fema.gov/media-library-data/20130726-1820-25045-6286/hzmh2_1_eq_tm.pdf (last accessed November 2017). For estimates on the economic impact of the February 2010 **M** 8.8 Chile earthquake, see the Organization for Economic Co-operation and Development (OECD) Economic Surveys at http://www.oecd-ilibrary.org/economics/oecd-economic-surveys-chile-2012_eco_surveys-chl-2012-en (last accessed November 2017). All of the datasets and models proposed here, as well as seismicity catalogs, a-values for background seismicity (agrids), the hazard input document (HID), source code input files, and results including hazard curves, hazard maps, deaggregation plots, risk and design values, can be found at ScienceBase (doi: 10.5066/F7WM1BK1).

Acknowledgments

Many international scientists from Regional Center for Seismology for South America (CERESIS), the 2016 U.S. Geological Survey (USGS)-University of Chile workshop, and reviewers provided information used in producing this model. The authors thank Global Earthquake Model (GEM) for providing their earthquake catalog and allowing us to view some preliminary information. The authors thank Susan Hoover for organizing the Costa Rica workshop, compiling presentations, and reviewing the article, and Sergio Barrientos for co-hosting this workshop. The authors especially appreciated discussions with Sergio Barrientos, Francisco Medina, Gavin Hayes, Jim Dewey, Carlos Costa, and Dan McNamara on seismic hazard issues. The authors benefited from reviews by Morgan Moschetti, Jill McCarthy, Ivan Wong, and several other anonymous reviewers. The authors thank United States Agency for International Development (USAID)-Office of U.S. Foreign Disaster Assistance (OFDA) for funding this analysis, and the 2016 USGS-University of Chile workshop held in Costa Rica.

References

Abrahamson, N. A., N. Gregor, and K. Addo (2016). BC Hydro ground motion prediction equations for subduction earthquakes, *Earthq. Spectra* **32,** 23–44.

Abrahamson, N. A., W. J. Silva, and R. Kamai (2014). Summary of the ASK14 ground motion relation for active crustal regions, *Earthq. Spectra* **30,** 1025–1055.

Allen, T. A., and D. J. Wald (2009). On the use of high-resolution topographic data as a proxy for seismic site conditions (V_{S30}), *Bull. Seismol. Soc. Am.* **99,** 935–943.

Alvarado, A., L. Audin, J. M. Nocquet, S. Lagreulet, M. Segovia, Y. Font, G. Lamarque, H. Yepes, P. Mothes, F. Rolandone, *et al.* (2014). Active tectonics in Quito, Ecuador, assessed by geomorphological studies, GPS data, and crustal seismicity, *Tectonics* **33,** 67–83.

American Society of Civil Engineers (ASCE) (2016). *Minimum Design Loads for Buildings and Other Structures, ASCE/SEI 7-16*, American Society of Civil Engineers, Reston, Virginia.

Atkinson, G. M. (2008). Ground-motion prediction equations for eastern North America from a referenced empirical approach—Implications for epistemic uncertainty, *Bull. Seismol. Soc. Am.* **98,** 1304–1318, doi: 10.1785/0120070199.

Atkinson, G. M., and D. M. Boore (2003). Empirical ground-motion relations for subduction-zone earthquakes and their application to Cascadia and other regions, *Bull. Seismol. Soc. Am.* **93,** 1703–1729.

Atkinson, G. M., and D. M. Boore (2006). Earthquake ground-motion prediction equations for eastern North America, *Bull. Seismol. Soc. Am.* **96,** 2181–2205, doi: 10.1785/0120050245.

Atkinson, G. M., and M. Macias (2009). Predicted ground motions for great interface earthquakes in the Cascadia subduction zone, *Bull. Seismol. Soc. Am.* **99,** 1552–1578.

Audemard, F. A., G. Romero, H. Rendon, and V. Cano (2005). Quaternary fault kinematics and stress tensors along the southern Caribbean from fault-slip data and focal mechanism solutions, *Earth Sci. Rev.* **69,** 181–233, doi: 10.1016/j.earscirev.2004.08.001.

Barrientos, S. E., and S. N. Ward (1990). The 1960 Chile earthquake: inversion for slip distribution from surface deformation, *Geophys. J. Int.* **103,** 589–598.

Beauval, C., H. Yepes, L. Audin, A. Alvarado, J.-M. Nocquet, D. Monelli, and L. Danciu (2014). Probabilistic seismic-hazard assessment in Quito, estimates and uncertainties, *Seismol. Res. Lett.* **85,** 1316–1327, doi: 10.1785/0220140036.

Beauval, C., H. Yepes, P. Palacios, M. Segovia, and A. Alvarado (2013). An earthquake catalog for seismic hazard assessment for Ecuador, *Bull. Seismol. Soc. Am* **103,** 773–786.

Bhaduri, B. L., E. A. Bright, P. R. Coleman, and J. E. Dobson (2002). LandScan: Locating people is what matters, *Geoinformatics* **5,** 34–37.

Bird, P. (2003). An updated digital model for plate boundaries, *Geochem. Geophys. Geosys.* **4,** no. 1027, 52, doi: 10.1029/2001GC000252.

Bondar, I., E. R. Engdahl, A. Villasenor, J. Harris, and D. Storchak (2015). ISC-GEM: Global Instrumental Catalogue (1900–2009), II. Location and seismicity patterns, *Phys. Earth Planet. In.* **239,** 2–13.

Boore, D. M. (2010). Orientation-independent, non geometric-mean measures of seismic intensity from two horizontal components of motion, *Bull. Seismol. Soc. Am.* **100,** 1830–1835.

Boore, D. M., J. P. Stewart, E. Seyhan, and G. M. Atkinson (2014). NGA-West2 equations for predicating PGA, PGV, and 5% damped PSA for shallow crustal earthquakes, *Earthq. Spectra* **30,** 1057–1085.

Building Seismic Safety Council (BSSC) (2015). NEHRP Recommended Seismic Provisions for New Buildings and Other Structures, Volume 1: Part 1 Provisions, Part 2 Commentary, FEMA P-1050-1, Washington, D.C., 555 pp.

Campbell, K. W. (2003). Prediction of strong ground motion using the hybrid empirical method and its use in the development of ground motion (attenuation) relations in eastern North America, *Bull. Seismol. Soc. Am.* **93,** 1012–1033.

Campbell, K. W., and Y. Bozorgnia (2014). NGA-West2 ground motion model for the average horizontal components of PGA, PGV, and 5% damped linear acceleration response spectra, *Earthq. Spectra* **30,** 1087–1115.

Chiou, B. S.-J., and R. Youngs (2014). Update of the Chiou and Youngs NGA model for the average horizontal component of peak ground motion and response spectra, *Earthq. Spectra* **30,** 1117–1153.

Cisternas, M., E. Garrett, R. L. Wesson, T. Dura, and L. L. Ely (2017). Unusual geologic evidence of coeval seismic shaking and tsunamis shows variability in earthquake size and recurrence in the area of the giant 1960 Chile earthquake, *Mar. Geol.* **385,** 101–113.

Cornell, C. A. (1968). Engineering seismic risk analysis, *Bull. Seismol. Soc. Am.* **58,** 1583–1606.

Costa, C., M. N. Machette, R. L. Dart, H. E. Bastias, J. D. Paredes, L. P. Perucca, G. E. Tello, and K. M. Haller (2000). Map and database of Quaternary faults and folds in Argentina, *U.S. Geol. Surv. Open-File Rept. 00-0108*, 81 p.

Costa, C. H., F. A. M. Audemard, F. H. R. Bezerra, A. Lavenu, M. N. Machette, and G. Paris (2006). An overview of the main Quaternary deformation of South America, *Rev. Asoc. Geol. Argent.* **61,** 461–479.

Dimate, C., L. Drake, H. Yepez, H. Rendon, G. Grunthal, and D. Giardini (1999). Seismic hazard assessment in the Northern Andes (PILOTO Project), *Ann. Geofisc.* **42,** 1039–1055.

Earle, P. S., D. J. Wald, K. S. Jaiswal, T. I. Allen, M. G. Hearne, K. D. Marano, A. J. Hotovec, and J. M. Fee (2009). Prompt Assessment of Global Earthquakes for Response (PAGER): A system for rapidly determining the impact of earthquakes worldwide, *U.S. Geol. Surv. Open-File Rept. 2009-1131*, 15 p.

Eguez, A., A. Alvarado, H. Yepes, M. N. Machette, C. Costa, and R. L. Dart (2003). Database and map of Quaternary faults and folds of Ecuador and its offshore regions, *U.S. Geol. Surv. Open-File Rept. 03-289*, 77 p.

Frankel, A., C. Mueller, T. Barnhard, D. Perkins, E. V. Leyendecker, N. Dickman, S. Hanson, and M. Hopper (1996). National seismic hazard maps—Documentation June 1996, *U.S. Geol. Surv. Open-File Rept. 96-532*, 110 p.

Gardner, J. K., and L. Knopoff (1974). Is the sequence of earthquakes in southern California, with aftershocks removed, Poissonian? *Bull. Seismol. Soc. Am.* **64,** 1363–1367.

Giardini, G., G. Grunthal, K. M. Shedlock, and P. Zhang (1999). The GSHAP global seismic hazard map, *Ann. Geofisc.* **42,** 1225–1228.

Gutenberg, B., and C. F. Richter (1944). Frequency of earthquakes in California, *Bull. Seismol. Soc. Am.* **34,** 185–188.

Haller, K. M., and R. Basili (2011). Developing seismogenic source models based on geologic fault data, *Seismol. Res. Lett.* **82,** 519–525.

Hayes, G. P., D. E. McNamara, L. Seidman, and J. Roger (2014). Quantifying potential earthquake and tsunami hazard in the Lesser Antilles subduction zone of the Caribbean region, *Geophys. J. Int.* **196,** 510–521, doi: 10.1093/gji/ggt385.

Hayes, G. P., D. J. Wald, and R. L. Johnson (2012). Slab 1.0: A three-dimensional model of global subduction zone geometries, *J. Geophys. Res.* **117,** no. B01302, doi: 10.1029/2011JB008524.

Idriss, I. M. (2014). An NGA-West2 empirical model for estimating the horizontal spectral values generated by shallow crustal earthquakes, *Earthq. Spectra* **30,** 1155–1177.

International Code Council (2015). *2015 International Building Code*, International Code Council, Falls Church, Virginia.

Jaiswal, K. S., and D. J. Wald (2010). An empirical model for global earthquake fatality estimation, *Earthq. Spectra* **26,** 1017–1037.

Jaiswal, K. S., and D. J. Wald (2011). Rapid estimation of the economic consequences of global earthquakes, *U.S. Geol. Surv. Open-File Rept. 2011–1116*, 47 p.

Jaiswal, K. S., D. Bausch, R. Chen, J. Bouabid, and H. Seligson (2015). Estimating annualized earthquake losses for the conterminous United States, *Earthq. Spectra* **31,** S221–S243, doi: 10.1193/010915EQS005M.

Jaiswal, K. S., M. D. Petersen, S. C. Harmsen, and G. M. Smoczyk (2014). Assessing the seismic risk potential of South America, *Second European Conf. on Earthquake Engineering and Seismology*, Istanbul, Turkey, 24–29 August 2014, Paper 1257.

Lavenu, A., R. Thiele, M. N. Machette, R. L. Dart, L-A. Bradley, and K. M. Haller (2000). Maps and database of Quaternary faults in Bolivia and Chile, *U.S. Geol. Surv. Open-File Rept. 00-283*, 50 p.

Luco, N., R. E. Bachman, C. B. Crouse, J. R. Harris, J. D. Hopper, C. A. Kircher, P. J. Caldwell, and K. S. Rukstales (2015). Updated to building-code maps for the 2015 NEHRP Recommended Seismic Provisions, *Earthq. Spectra* **31,** S245–S27.

Luco, N., B. R. Ellingwood, R. O. Hamburger, J. D. Hooper, J. K. Kimball, and C. A. Kircher (2007). Risk-targeted versus current seismic design maps for the conterminous United States, *Proc. of the Structural Engineers Association of California 76th Annual Convention*, Lake Tahoe, California, 27–28 September 2007.

Macharé, J., C. H. Fenton, M. N. Machette, A. Lavenu, C. Costa, and R. L. Dart (2003). Database and map of Quaternary faults and folds in Perú and its offshore region, *U.S. Geol. Surv. Open-File Rept. 03-451*, 55 p.

McCann, W. R (2006). Estimating the threat of tsunamigenic earthquake and earthquake induced-landslide tsunami in the Caribbean, in *Caribbean Tsunami Hazard*, A. Mercado-Irizarry and P. L. F. Liu (Editors), World Scientific Publishing Company, Singapore, 43–65.

Medina, F., S. C. Harmsen, and S. E. Barrientos (2017). Probabilistic seismic hazard analysis for Chile, *16th World Conf. on Earthquake Engineering*, Santiago, Chile, 9–13 January 2017, Paper 2994.

Moschetti, M. P., P. M. Powers, M. D. Petersen, O. S. Boyd, R. Chen, E. H. Field, A. D. Frankel, K. M. Haller, S. C. Harmsen, C. S. Mueller, and R. L. Wheeler (2015). Seismic source characterization for the 2014 update of the U.S. national seismic hazard model, *Earthq. Spectra* **31,** S31–S57.

Pagani, M., D. Monelli, H. Crowley, L. Danciu, E. H. Field, S. Wiemer, and D. Giardini (2010). GEM1 hazard: Description of input models, calculation engine and main results, *GEM Tech. Rept. 2010-3*, GEM Foundation, Pavia, Italy.

Papazachos, B. C., E. M. Scordilis, C. B. Panagiotopoulus, and G. F. Karakaisis (2004). Global relations between seismic fault parameters and moment magnitude of earthquakes, *Bull. Geol. Soc. Greece* **36,** 1482–1489.

París, G., M. N. Machette, R. L. Dart, and K. M. Haller (2000). Map and database of Quaternary faults and folds in Colombia and its offshore regions, *U.S. Geol. Surv. Open-File Rept. 00-0284*, 66 p.

Petersen, M. D., A. D. Frankel, S. C. Harmsen, C. S. Mueller, K. M. Haller, R. L. Wheeler, R. L. Wesson, Y. Zeng, O. S. Boyd, D. M. Perkins, *et al.* (2008). Documentation for the 2008 update of the United States National Seismic Hazard Maps, *U.S. Geol. Surv. Open-File Rept. 2008-1128*, 61 pp.

Petersen, M. D., S. C. Harmsen, C. S. Mueller, K. M. Haller, K. S. Jaiswal, and K. S. Rukstales (2017). Sensitivity study of seismic hazard and risk for the continent of South America, *16th World Conf. on Earthquake Engineering*, Santiago Chile, 9–13 January 2017.

Petersen, M. D., M. P. Moschetti, P. M. Powers, C. S. Mueller, K. M. Haller, A. D. Frankel, Y. Zeng, S. Razaeian, S. C. Harmsen, O. S. Boyd, *et al.* (2014). Documentation for the 2014 update of the United States National Seismic Hazard Maps, *U.S. Geol. Surv. Open-File Rept. 2014-1091*, 243 pp.

Petersen, M. D., M. P. Moschetti, P. M. Powers, C. S. Mueller, K. M. Haller, A. D. Frankel, Y. Zeng, S. Rezaeian, S. C. Harmsen, O. S. Boyd, *et al.* (2015). The 2014 United States National Seismic Hazard Model, *Earthq. Spectra* **31,** S1–S30.

Pezeshk, S., A. Zandieh, and B. Tavakoli (2011). Hybrid empirical ground-motion prediction equations for eastern North America using NGA models and updated seismological parameters, *Bull. Seismol. Soc. Am.* **101,** 1859–1870, doi: 10.1785/0120100144.

Rezaeian, S., M. D. Petersen, and M. P. Moschetti (2015). Ground motion models used in the 2014 US National Seismic Hazard Maps, *Earthq. Spectra* **31,** S59–S84.

Saadi, A., M. N. Machette, K. M. Haller, R. L. Dart, L-A. Bradley, and A. M. P. D. de Souza (2002). Map and database of Quaternary faults and lineaments in Brazil, *U.S. Geol. Surv. Open-File Rept. 02-230*, 63 p.

Seyhan, E., and P. S. Stewart (2014). Semi-empirical nonlinear site amplification from NGA-West2 data and simulations, *Earthq. Spectra* **30,** 1241–1256, doi: 10.1193/063013EQS181M.

Shedlock, K. M. (1999). Seismic hazard map of North and Central America and the Caribbean, *Ann. Geofisc.* **42,** 977–997.

Shedlock, K. M., and J. G. Tanner (1999). Seismic hazard map of the western hemisphere, *Ann. Geofisc.* **42,** 1199.

Silva, V., K. S. Jaiswal, G. Weatherill, and H. Crowley (2014). Global assessment of human losses due to earthquakes, *Second European Conf. on Earthquake Engineering and Seismology*, Istanbul, Turkey, 24–29 August 2014.

Silva, W., N. Gregor, and R. Darragh (2002). Development of regional hard rock attenuation relations for central and eastern North America, *Pacific Engineering and Analysis Technical Report*, 57 p.

Strasser, F. O., M. C. Arango, and J. J. Bommer (2010). Scaling of the source dimensions of interface and intraslab subduction-zone earthquakes with moment magnitude, *Seismol. Res. Lett.* **81,** 941–950.

Sykes, L. R., W. R. McCann, and A. L. Kafka (1982). Motion of Caribbean plate during last 7 million years and implications for earlier Cenozoic movements, *J. Geophys. Res.* **87,** 10,656–10,676.

Tanner, J. G., and J. B. Shepherd (1997). Seismic hazard in Latin America and the Caribbean: Volume 1, Project catalogue and seismic hazard maps, *Instituto Panamericano de Geografia y Historia Final Report, Project No. 89–0190*.

Tavakoli, B., and S. Pezeshk (2005). Empirical-stochastic ground-motion prediction for eastern North America, *Bull. Seismol. Soc. Am.* **95,** 2283–2296.

Tavera, H., L. Rodriguez, and C. Condori (2015). Evaluacion del Peligro Sismico en America del Sur, in *Informe Tecnico Preliminar*, CERESIS, 20 pp. (in Spanish).

Toro, G. R. (2002). Modification of the Toro *et al.* (1997) attenuation equations for large magnitudes and short distances, *Risk Engineering Technical Report*, 10 pp.

Toro, G. R., N. A. Abrahamson, and J. F. Schneider (1997). Model of strong ground motions from earthquake in central and eastern North America —Best estimates and uncertainties, *Seismol. Res. Lett.* **68,** 41–57.

U.S. Department of Defense (2016). *Unified Facilities Criteria: Structural Engineering, UFC 3-301-01*, U.S. Department of Defense, Washington, D.C., 162 pp.

Wald, D. J., P. S. Earle, T. I. Allen, K. Jaiswal, K. Porter, and M. Hearne (2008). October, Development of the U.S. Geological Survey's PAGER system (prompt assessment of global earthquakes for response), *Proc. of the 14th World Conf. on Earthquake Engineering*, Istanbul, Turkey, 24–29 August 2014.

Weichert, D. H. (1980). Estimation of the earthquake recurrence parameters for unequal observation periods for different magnitudes, *Bull. Seismol. Soc. Am.* **70,** 1337–1346.

Worden, C. B., M. C. Gerstenberger, D. A. Rhoades, and D. J. Wald (2012). Probabilistic relationships between ground-motion parameters and modified Mercalli intensity in California, *Bull. Seismol. Soc. Am.* **102,** 204–221.

Zhao, J. X., J. Zhang, A. Asano, Y. Ohno, T. Oouchi, T. Takahashi, H. Ogawa, K. Irikura, H. K. Thio, P. G. Somerville, *et al.* (2006). Attenuation relations of strong ground motion in Japan using site classification based on predominant period, *Bull. Seismol. Soc. Am.* **96,** 898–913.

U.S. Geological Survey
Geologic Hazards Science Center
Denver Federal Center
P.O. Box 25046, MS 966
Denver, Colorado 80225
mpetersen@usgs.gov

Manuscript received 3 January 2017;
Published Online 16 January 2018